Research Article

Jean-François Ganghoffer*, Rachid Rahouadj, Julien Boisse and Samuel Forest

Phase field approaches of bone remodeling based on TIP

DOI: 10.1515/jnet-2015-0048
Received July 26, 2015; revised November 13, 2015; accepted December 1, 2015

Abstract: The process of bone remodeling includes a cycle of repair, renewal, and optimization. This adaptation process, in response to variations in external loads and chemical driving factors, involves three main types of bone cells: osteoclasts, which remove the old pre-existing bone; osteoblasts, which form the new bone in a second phase; osteocytes, which are sensing cells embedded into the bone matrix, trigger the aforementioned sequence of events. The remodeling process involves mineralization of the bone in the diffuse interface separating the marrow, which contains all specialized cells, from the newly formed bone. The main objective advocated in this contribution is the setting up of a modeling and simulation framework relying on the phase field method to capture the evolution of the diffuse interface between the new bone and the marrow at the scale of individual trabeculae. The phase field describes the degree of mineralization of this diffuse interface; it varies continuously between the lower value (no mineral) and unity (fully mineralized phase, e.g. new bone), allowing the consideration of a diffuse moving interface. The modeling framework is the theory of continuous media, for which field equations for the mechanical, chemical, and interfacial phenomena are written, based on the thermodynamics of irreversible processes. Additional models for the cellular activity are formulated to describe the coupling of the cell activity responsible for bone production/resorption to the kinetics of the internal variables. Kinetic equations for the internal variables are obtained from a pseudo-potential of dissipation. The combination of the balance equations for the microforce associated to the phase field and the kinetic equations lead to the Ginzburg–Landau equation satisfied by the phase field with a source term accounting for the dissipative microforce. Simulations illustrating the proposed framework are performed in a one-dimensional situation showing the evolution of the diffuse interface separating new bone from marrow.

Keywords: Bone remodeling, phase field, thermodynamics of irreversible processes, diffuse interface, Ginzburg–Landau equation, cellular activity

1 Introduction

Bone tissue is an adaptable living structure, having the capacity to adapt its internal structure and external shape to variations in its mechanical environment. Bone is a complex multiscale structure as shown in Figure 1, with two distinct types of tissues: the cortical bone, which is dense and compact and forms the outer surface of bones, and it encloses the trabecular bone tissue, which has a honeycomb-like structure and is made of trabeculae surrounded by bone marrow. The mineralized matrix of bone tissue has an organic component consisting mainly of type I collagen and an inorganic component of bone mineral made up of various salts.

***Corresponding author: Jean-François Ganghoffer:** LEMTA, Université de Lorraine, 2 Avenue de la Forêt de Haye, TSA 60604, 54518 Vandœuvre-lès-Nancy cedex, France, e-mail: jean-francois.ganghoffer@univ-lorraine.fr
Rachid Rahouadj, Julien Boisse: LEMTA, Université de Lorraine, 2 Avenue de la Forêt de Haye, TSA 60604, 54518 Vandœuvre-lès-Nancy cedex, France, e-mail: rachid.rahouadj@univ-lorraine.fr, julien.boisse@univ-lorraine.fr
Samuel Forest: MINES ParisTech, Centre des Matériaux, CNRS UMR 7633, BP 87, 91003 Evry cedex, France, e-mail: samuel.forest@mines-paristech.fr

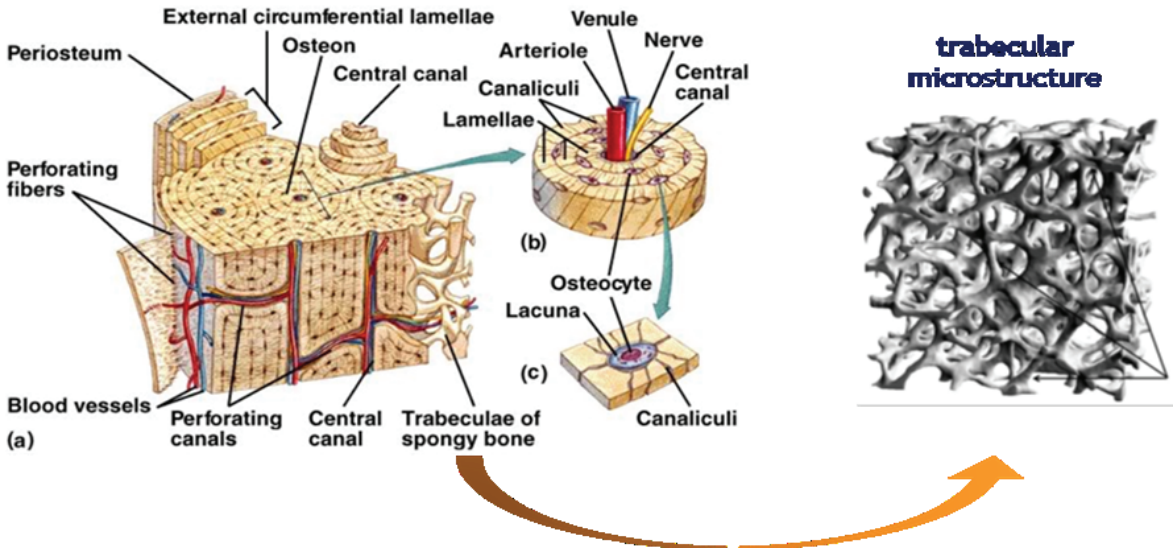

Figure 1. Histological description of trabecular and cortical bone. Trabecular bone is made of skeleton (80%) and has an open cell porous structure. The cortical region is compact (20%) and contains lamellae of collagen fibers, with sensing cells trapped between the stratified layers (osteocytes) and other cells communicating by tubules through the collagen matrix.

Bone is a dynamic living tissue, with the ability to modify its internal architecture in response to its environment in order to maintain its structural integrity as the support of the body and its physiological functions, especially as a reservoir of nutrients [1, 2].

In adult bones, skeletal development is the result of growth, modeling, and remodeling processes. Growth means the change of overall bone mass and is due to both genetic and epigenetic factors, including mechanical physiological loads supported by the body. Modeling occurs in a concomitant manner to growth, as it modulates the bone architecture during growth in response to a variation of the mechanical conditions. It accordingly controls the shape, size, and strength of bones by the addition or resorption of bone material at the surfaces of trabeculae. Remodeling involves the replacement of old bone by new lamellar bone through resorption processes; bone remodeling as an integrated process incorporates the mechanisms through which living bone adapts its internal structure to changes of the external load. The gold standard for bone remodeling is the BMU, the acronym for basic multicellular unit [3].

Both cortical and trabecular bone undergo remodeling, the difference between them being in the geometrical progression: the BMU has the ability to move along the surface of the trabeculae, whereas it penetrates the compact cortical bone by digging a tunnel. The temporal sequence of remodeling steps on a trabecula is illustrated in Figure 2.

Bone remodeling plays an important role in the processes of formation, maintenance, and repair of bone tissues; it aims at shaping the skeleton and repairing bone fractures by adapting the microstructure in response to mechanical and physiological stimuli: following a phase of growth and development, bone undergoes a continuous cycle of repair, renewal, and optimization in which mechanical stimuli play a fundamental role. Bone remodeling can also be perturbed in a pathological manner, due to age-related factors, changes in physical activity, drugs, secondary diseases, menopause-associated hormonal changes, all leading to an imbalance of the extracellular matrix remodeling and local angionesis.

Bone remodeling is further classified as either internal or external bone remodeling [4, 5]: external remodeling occurs by apposition or resorption of new bone on the external surfaces and is thus also called surface remodeling. It is opposite to internal remodeling, which only occurs at the scale of individual trabeculae, leading to an overall density change. An increase in mechanical stimuli is found to cause bone formation, whereas a decrease in load leads to bone resorption [6]. Bone undergoes a continuous and repetitive remodeling cycle involving the sequence of activation, resorption of old bone (modeling), inversion, and formation of new bone (remodeling) by specialized cells (osteoclasts/osteoblasts/osteocytes), as illustrated on the

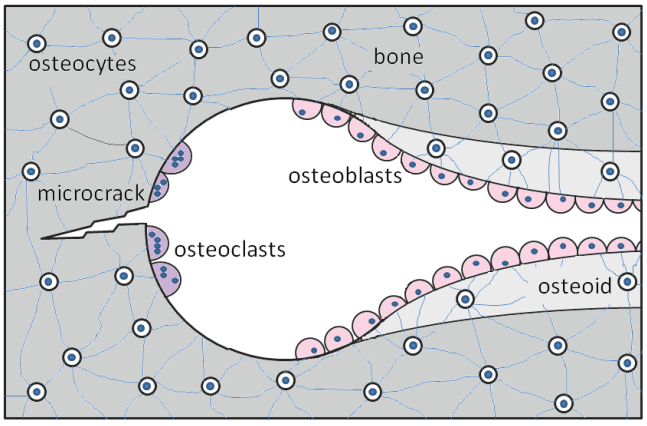

Figure 2. Schematic view of a BMU moving along a microcrack within trabecular bone. Osteoclasts resorb bone in the form of a cutting cone. Osteoblasts subsequently fill the resorbed space with osteoid (the new bone matrix) and differentiate into sensing cells called osteocytes.

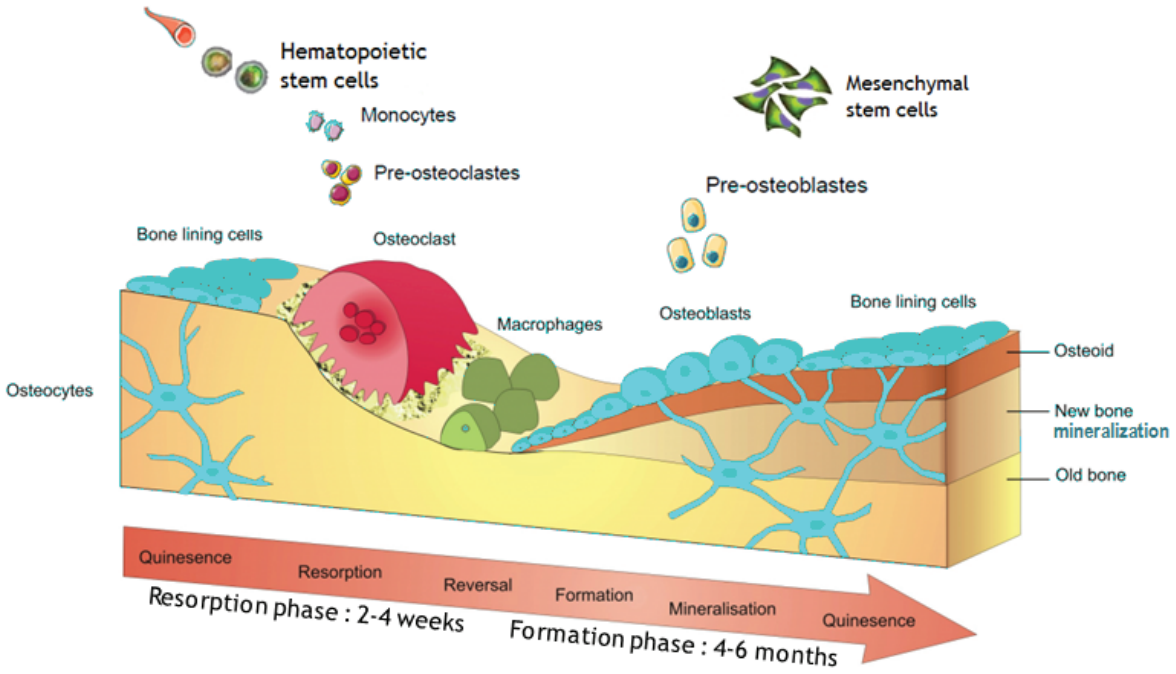

Figure 3. Bone remodeling cycle. From Biomedical Tissue Research, University of York; www.york.ac.uk/res/bonefromblood; figure completed by the delivery of cells.

synthetic Figure 3. In the remodeling process, specialized cells called osteoclasts resorb bone tissue, whereas other cells called osteoblasts deposit new bone tissue. When osteoblasts become trapped within the bone matrix they secrete, they differentiate into osteocytes, playing the role of load sensing cells. Osteoblasts increase bone mass under high loading conditions, by producing hydroxyapatite, the mineral forming the new bone, together with collagen I, an organic matrix. Bone tissue is removed by osteoclasts under low loading conditions; the overall cell activity aims to reach an optimized bone architecture. The interactions between the activity of osteoblasts and osteoclasts is responsible for bone remodeling at the level of the BMU.

Many biological factors are involved in the regulation of the bone remodeling process [7, 8], including autocrine and paracrine signaling molecules, systemic hormones and extracellular matrix components that affect cell-to-cell communication, migration, adhesion, proliferation, and differentiation. The interactions between osteoclasts and osteoblasts are very complex because osteoblasts can regulate the activity of os-

teoblasts by specialized molecules called RANK and RANKL (see [9] for a review). More details relative to the biological aspects of bone remodeling will be given in Section 6.

The integrity and strength of the bone microstructure is determined by the balance between the volume of resorbed bone and that of newly formed bone [10, 11]. One can classify the models developed in the literature aiming at simulating the functional adaptation of bone into three main classes: optimization theories considering bone as a mechanical structure undergoing an evolutionary process, phenomenological models, and mechanistic models, some of which in this third category incorporate the chemical and biological processes responsible for the modification of bone architecture. More details relative to each of these classes of models are given in [12].

The need for bone remodeling models and simulations is especially marked in applications dealing with bone adaptivity, such as bone implants and scaffold design [13]. This contribution focuses on the bone internal remodeling processes occurring at the scale of individual trabeculae, to refine the more external remodeling approaches [14, 15].

As proposed in [16], remodeling models can be classified into several categories: (i) models based on the global optimality criterion [17–21]; (ii) models including a homeostatic state of mechanical energy [22–36]; (iii) models based on damage [26, 27, 37, 38]; (iv) models including both mechanical and metabolic factors in the remodeling cycle [39–45]; (v) one model considering the interstitial fluid flow [46]; and (vi) models based on a reaction diffusion and including mechanical stress but without biophysical activities of osteoblasts and osteoclasts [47–50].

To complete the picture, one shall also consider mathematical models describing the activity of BMUs and based on the work of Komarova et al. [51] focusing on the non-linear autoregulation between osteoblasts and osteoclasts [52–57]. The interactions with biological factors highlighted by Komarova et al. [51] were completed by Bonfoh et al. [58], who considered the influence of mechanical stimuli on cell dynamics. More recently, Hambli [16] proposed an approach that combined the work of Komarova et al. [51] and Bonfoh et al. [58] to include fatigue damage growth and repair, mineralization, porosity, bone properties evolution, and cellular accommodation during the load history.

As a main originality advocated in the present contribution, we shall set up mechanobiological descriptions of bone remodeling at the trabecular level, considering a field theoretical approach within the thermodynamics of irreversible processes (TIP). Thereby, we shall set up a multiphysical framework incorporating mechanical, chemical, diffusion phenomena, and the mineralization of the osteoid apposed on the existing bone. Furthermore, we shall provide a micromechanical view of the interface propagation between marrow and new bone, by incorporating a scalar phase field variable representing the proportion of mineralized bone. These field equations will, in a last stage of the model, be coupled with the cellular activity responsible for bone remodeling phenomena.

The phase field theory is designed for the continuum modeling of diffuse interface migration and therefore is a good candidate for field modeling of bone remodeling processes [59]. The phase field approach has recently been applied to the growth of tumors but not yet to bone remodeling [60].

This paper is organized as follows: The bone remodeling cycle is described from the point of view of physiology and biology in Section 2. The field equations reflecting the interactions amongst these phenomena shall be expressed based on the principle of virtual power, highlighting macroscopic and microscopic forces (Section 3). The energy balance and the local dissipation are expressed in Section 4, together with the state laws, the kinetic equations for the internal variables, and the spatio-temporal evolution of the phase field, so-called Ginzburg–Landau equation. The set of governing equations is finally obtained based on the specification of the different contributions to the free energy density (Section 5). The issue of the connection between the cellular activity and the mechanical stimuli sensed by the osteocytes network is addressed in Section 6. The formation of new bone is illustrated numerically in a one-dimensional (1D) example in Section 7. Finally, a summary of the main thrust of the paper is given (Section 8) together with a few perspectives for future research.

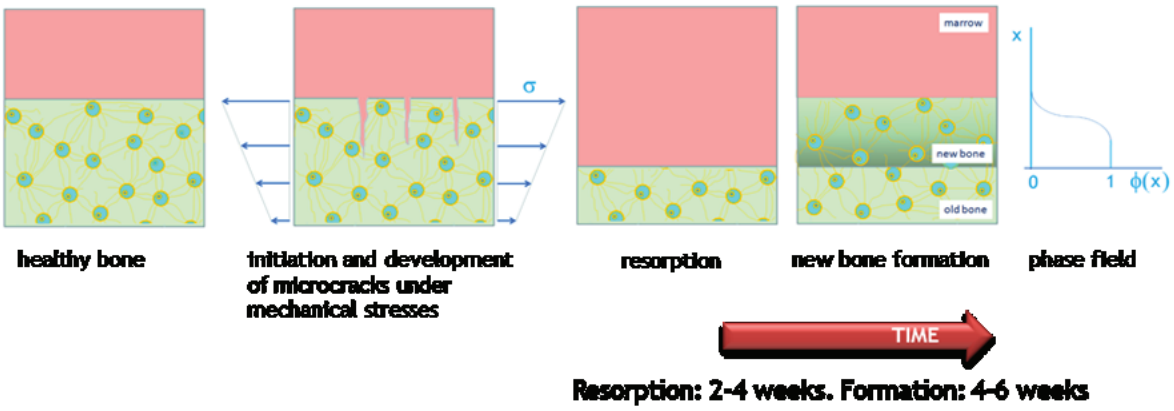

Figure 4. Schematic remodeling cycle including four main steps: healthy bone, initiation and development of microcracks under mechanical stresses, resorption, and new bone formation. The evolution of the phase order parameter is represented in 1D as a function of variable x.

2 Schematic bone remodeling cycle

Following a phase of growth and development, bone undergoes a continuous cycle of repair, renewal, and optimization in which mechanical stimuli play a fundamental role. The various stages of remodeling are summarized in Figure 2, showing the corresponding activity of specialized cells. The first stage of the cycle is activation: under the action of repeated stimuli, such as strain energy, stress concentrations, high strain levels, and existing microcracks, mechanical signals are detected by the osteocytes forming a network within the available space between successive bone lamellae. The osteocytes then send a signal to the osteoclasts, which erode the matrix to resorb old bone. This is followed by the formation of osteoid, a non-mineralized organic portion of the bone matrix forming prior to the maturation of bone tissue. Mineralization resulting from the activity of osteoblasts then proceeds by the synthesis of an extracellular matrix, composed of 90% collagen fibers, 10% proteoglycans, and non-collagen proteins involved in the regulation of mineralization. New bone consists of hydroxyapatite, the mineral phase, the dissolution of which has the following chemical reaction (bone formation corresponds to the inverse reaction), which condenses a more complicated set of (up to 14) chemical reactions:

$$[Ca_3(Po_4)_2]_3Ca(OH)_2 + 8H^+ \rightarrow 10Ca^{2+} + 6HPO_4^{2-} + 2H_2O.$$

Because of the complexity of bone remodeling mechanisms, we shall consider a small representative volume of material from the standpoint of physicochemical/biochemical mechanisms and mechanical phenomena, as illustrated in the simplified view depicted in Figure 4. In the present work, we shall consider mechanical factors as the main stimuli triggering bone remodeling: due to the formation and development of microcracks under mechanical stresses, strain energy builds up, leading to stress concentration around the crack tips (Figure 4). The existing bone needs first to be eroded to remove the stress concentration zones (modeling process), before new bone can be formed to shape the eroded trabeculae close to their original trabecular shape (remodeling process).

3 Phase field modeling: Virtual power principle and balance equations

It is assumed that the degrees of freedom (DOFs) of the thermodynamic system shown in Figure 3 can be resumed to the order parameter ϕ, its gradient $\nabla\phi$, the gradient of the displacement ∇u, the total number of moles k-species n_k, and temperature T, all encapsulated into the vector of DOF, $\{\phi, \nabla\phi, \nabla u, n_k, T\}$. Its gra-

dient rapidly varies in the diffuse interface between bone and marrow and contributes to the corresponding interface energy. The phase field describes the degree of mineralization within newly formed bone (the degree of formation of new bone due to the mineralization of the produced species); a number of authors [16, 39] introduced different models for the ash function denoting the degree of mineralization.

The total number of moles n_k results from the production of the corresponding chemical species by chemical reactions n_k^{prod} and of exchanges with the external environment n_k^{exch} (in the present case, the bone marrow) as expressed in the balance law:

$$n_k = n_k^{\text{exch}} + n_k^{\text{prod}}.$$

The principle of virtual power states that the sum of the virtual power of internal, external, and contact forces vanishes in a quasi-static situation (one shall add the virtual power of inertia forces for non-quasi-static situations):

$$\int_V p^{(i)} dV + \int_V p^{(e)} dV + \int_{\partial V} p^{(c)} dS = 0.$$

The previous integrals have been formulated as volume integrals of the corresponding densities over a fixed control volume V. This formulation based on an extended principle of virtual power was proposed by Ammar et al. [61] as a generalization of Gurtin's thermodynamic phase field model, which introduces additional balance equations for generalized so-called microforces and microstresses in the context of phase transformation [62, 63].

Previous weak form of equilibrium relies on power densities involving the rates of the DOF and their conjugated variables

$$\begin{aligned} p^{(i)} &= \pi_\phi \dot{\phi} - \xi_\phi \cdot \nabla\dot{\phi} - \sigma : \nabla\dot{\mathbf{u}} + \mu_k^{\text{prod}} \dot{n}_k^{\text{prod}}, \\ p^{(e)} &= \pi_\phi^{\text{ext}} \dot{\phi} + \mathbf{f} \cdot \dot{\mathbf{u}} + \mu_k^{\text{prodext}} \dot{n}_k^{\text{prod}}, \\ p^{(c)} &= \pi_\phi^{\text{cont}} \dot{\phi} + \mathbf{t} \cdot \dot{\mathbf{u}} + \mu_k^{\text{prodcont}} \dot{n}_k^{\text{prod}}, \end{aligned}$$

where π_ϕ, π_ϕ^{ext} and π_ϕ^{cont} represent the internal, external, and contact forces associated to ϕ, respectively, ξ_ϕ is the microforce associated to $\nabla\phi$, and σ is the Cauchy stress tensor. The scalars μ_k^{prod}, μ_k^{prodext} and μ_k^{prodcont} are the chemical potentials (for the production, external, and contact chemical actions, respectively) associated to the production term n_k^{prod}, and $\mathbf{f}$ and $\mathbf{t}$ denote the volume and surface densities of external forces, respectively.

The free energy may be expressed as $\Psi(\phi, \nabla\phi, \epsilon^e, n_k^{\text{exch}}, T)$, where ϵ^e is the elastic part of the total strain; by analogy with elasticity, it incorporates the number of moles being exchanged.

The equilibrium equations arising from the principle of virtual powers are therefore of the following local form in V:

$$\begin{aligned} \nabla \cdot \boldsymbol{\sigma} + f &= 0, \\ \nabla \cdot \boldsymbol{\xi}_\phi + \pi_\phi^{\text{ext}} + \pi_\phi &= 0, \qquad (3.1) \\ (\mu_k^{\text{prod}} + \mu_k^{\text{prodext}}) \dot{n}_k^{\text{prod}} &= 0, \qquad (3.2) \end{aligned}$$

with the decomposition of the mole fraction of k-species into exchanged and produced terms, viz. $\dot{n}_k = \dot{n}_k^{\text{exch}} + \dot{n}_k^{\text{prod}}$, which implies the condition $\mu_k^{\text{prodcont}} \dot{n}_k^{\text{prod}} = 0$, together with the boundary conditions on ∂V for the stress field and the microforce equations, respectively,

$$\boldsymbol{\sigma} \cdot \mathbf{n} = \mathbf{t}, \quad \boldsymbol{\xi}_\phi \cdot \mathbf{n} = \pi_\phi^{\text{cont}}.$$

These boundary conditions are supplemented by boundary conditions for the thermal variables ($\mathbf{q}$, T). The following choices are made with respect to external fields:

$$\begin{aligned} \pi_\phi^{\text{ext}} &= 0, \qquad (3.3) \\ \mu_k^{\text{prod}} + \mu_k^{\text{prodext}} &= 0. \end{aligned}$$

Thereby, the external force associated to the phase field vanishes, whereas the chemical potential of external forces is balanced by the internal chemical potential.

4 A thermodynamic framework for a phase field approach of bone remodeling

The TIP is the adequate framework to formulate the internal dissipation accounting for the multiphysical processes underlying bone remodeling: mechanical dissipation, chemical reactions, and transport phenomena of the produced chemical species. From a constitutive point of view, bone is modeled as an elastic orthotropic solid material undergoing small strains; the constitutive law of the bulk material can be obtained by the homogenization of the underlying microstructure, based on an idealized prototype architecture [64].

4.1 Energy balance

The combination of the first principle and the virtual power principle allows obtaining the energy balance on the basis of the expression of free energy rate as follows:

$$\begin{aligned}
\dot{\Psi} &= \partial_{\phi}\Psi\dot{\phi} + \partial_{\nabla\phi}\Psi\cdot\nabla\dot{\phi} + \partial_{\epsilon^e}\Psi\colon\dot{\epsilon}^e + \partial_{n_k^{\text{exch}}}\Psi\dot{n}_k^{\text{exch}} + \partial_t\Psi\dot{T},\\
\dot{E} &= -P^{(i)} + \delta Q,\\
\dot{e} &= -\pi_{\phi}\dot{\phi} + \xi_{\phi}\cdot\nabla\dot{\phi} + \sigma\colon\nabla\dot{u} - \mu_k^{\text{prod}}\dot{n}_k^{\text{prod}} - \nabla\cdot\mathbf{q},\\
T\dot{s} &= \dot{e} - \dot{T}s - \dot{\Psi}.
\end{aligned}$$

The last expression combined with the second principle, inequality

$$\dot{s} \geq -\nabla\cdot\left(\frac{q}{T}\right) + \frac{1}{T}\nabla\cdot(\mu_k^{\text{prod}}J_k)$$

leads to Clausius–Duhem inequality,

$$\begin{aligned}
&-\pi_{\phi}\dot{\phi} + \xi_{\phi}\dot{\nabla}\dot{\phi} + \boldsymbol{\sigma}\colon\nabla\dot{\mathbf{u}} - \mu_k^{\text{prod}}\dot{n}_k^{\text{prod}} - \nabla.\mathbf{q} - \dot{T}s - \partial_{\phi}\Psi\dot{\phi} - \partial_{\nabla\phi}\Psi\cdot\nabla\dot{\phi} - \partial_{\boldsymbol{\epsilon}^e}\Psi\colon\dot{\boldsymbol{\epsilon}}\\
&\quad - \partial_{n_k^{\text{exch}}}\Psi\dot{n}_k^{\text{exch}} - \partial_T\Psi\dot{T} + T\nabla\cdot\left(\frac{\mathbf{q}}{T}\right) - \nabla\cdot(\mu_k^{\text{prod}}\mathbf{J}_k) \geq 0.
\end{aligned}$$

The last inequality can be reorganized as follows:

$$\begin{aligned}
&[-\pi_{\phi} - \partial_{\phi}\Psi]\dot{\phi} + [\xi_{\phi} - \partial_{\nabla\phi}\Psi]\cdot\nabla\dot{\phi} + [\boldsymbol{\sigma} - \partial_{\boldsymbol{\epsilon}^e}\Psi]\colon\dot{\boldsymbol{\epsilon}}^e + \boldsymbol{\sigma}\colon\dot{\boldsymbol{\epsilon}}^{\text{irr}} - \mu_k^{\text{prod}}\dot{n}_k^{\text{prod}}\\
&\quad - \partial_{n_k^{\text{exch}}}\dot{n}_k^{\text{exch}} - \nabla\cdot(\mu_k^{\text{prod}}\mathbf{J}_k) - [s + \partial_T\Psi]\dot{T} - \left(\frac{1}{T}\right)q\cdot\nabla T \geq 0.
\end{aligned} \tag{4.1}$$

Anticipating the identification of the state laws, the previous inequality leads to the total dissipation:

$$-\pi_{\phi}^{\text{diss}}\dot{\phi} + \boldsymbol{\sigma}\colon\dot{\boldsymbol{\epsilon}}^{\text{irr}} - \mu_k^{\text{prod}}\dot{n}_k^{\text{prod}} - \partial_{n_k^{\text{exch}}}\Psi\dot{n}_k^{\text{exch}} - \nabla\cdot(\mu_k^{\text{prod}}\mathbf{J}_k) - \left(\frac{1}{T}\right)\mathbf{q}\cdot\nabla T \geq 0.$$

Thus, the residual dissipation takes the final form

$$-\pi_{\phi}^{\text{diss}}\dot{\phi} + \boldsymbol{\sigma}\colon\dot{\boldsymbol{\epsilon}}^{\text{irr}} - \mu_k^{\text{prod}}\dot{n}_k^{\text{prod}} - \mathbf{J}_k\cdot\nabla\mu_k^{\text{prod}} - \left(\frac{1}{T}\right)q\cdot\nabla T \geq 0.$$

The different sources of dissipation associated with the phase field, mechanical, chemical, and thermal phenomena are, respectively,

$$D_{\phi} = -\pi_{\phi}^{\text{diss}}\dot{\phi}, \quad D_{\text{mech}} = \boldsymbol{\sigma}\colon\dot{\boldsymbol{\epsilon}}^{\text{irr}}, \quad D_{\text{chem}} = -\mu_k^{\text{prod}}\dot{n}_k^{\text{prod}} - \mathbf{J}_k\cdot\nabla\mu_k^{\text{prod}}, \quad D_{\text{therm}} = -\mathbf{q}\cdot\left(\frac{\nabla T}{T}\right).$$

4.2 State laws

The state laws are conventionally obtained from the Clausius–Duhem inequality (4.1) by the standard Colleman–Noll procedure (the rates factoring the quantities under brackets in (4.1) have arbitrary signs),

$$\begin{aligned}
\xi_{\phi} &= \partial_{\nabla\phi}\Psi,\\
\pi_{\phi}^{\text{nondiss}} &= -\partial_{\phi}\Psi,
\end{aligned} \tag{4.2}$$

where the internal phase field force decomposes additively into

$$\pi_\phi = \pi_\phi^{\text{nondiss}} + \pi_\phi^{\text{diss}},$$

with the dissipative microforce, Cauchy stress, chemical potential, and entropy density, respectively, given by

$$\pi_\phi^{\text{diss}} = \pi_\phi + \partial_\phi \Psi, \tag{4.3}$$

$$\boldsymbol{\sigma} = \partial_{\epsilon^e} \Psi,$$

$$\mu_k^{\text{prod}} = \partial_{n_k^{\text{exch}}} \Psi, \tag{4.4}$$

$$s = -\partial_T \Psi.$$

4.3 Kinetic laws

At this stage of the modeling, one needs to specify the kinetic laws that govern the evolution of the internal variables. For this objective, one introduces a scalar valued dissipation function $\Omega(\pi_\phi^{\text{diss}}, \boldsymbol{\sigma}, \nabla\mu_k^{\text{prod}}, \mu_k^{\text{prod}}, \nabla T)$ decomposing into different contributions involving the forces satisfying the previous state laws,

$$\Omega = \frac{1}{2} L(\phi) \nabla\mu_k^{\text{prod}} \cdot \nabla\mu_k^{\text{prod}} - \frac{1}{2}\left(\frac{1}{\tau_\phi}\right)(\pi_\phi^{\text{diss}})^2 + f(\boldsymbol{\sigma}) - \frac{1}{2}\left(\frac{1}{\tau_k}\right)(\mu_\phi^{\text{prod}})^2 + \frac{1}{2} k \left(\frac{\nabla T}{T}\right)^2 \tag{4.5}$$

and satisfying Onsager's properties. As expected, the resulting kinetic laws follow from previous writing as

$$\dot{\boldsymbol{\epsilon}}_{\text{mech}}^{\text{irr}} = \frac{\partial \Omega}{\partial \boldsymbol{\sigma}} = \dot{\lambda} \frac{\partial f}{\partial \boldsymbol{\sigma}},$$

$$\dot{\phi} = -\frac{\partial \Omega}{\partial \pi_\phi^{\text{diss}}} = -\frac{1}{\tau_\phi} \pi_\phi^{\text{diss}},$$

$$\dot{n}_k^{\text{prod}} = \frac{\partial \Omega}{\partial \mu_k^{\text{prod}}} = -\frac{1}{\tau_k} \mu_k^{\text{prod}}, \tag{4.6}$$

$$-\mathbf{J}_k = \frac{\partial \Omega}{\partial \nabla_k^{\text{prod}}} = L(\phi) \nabla\mu_k^{\text{prod}}, \tag{4.7}$$

where the variable $\dot{\lambda}$ is the plastic multiplier. The influence function $L(\phi)$ relating the mass flux of chemical species to the gradient of the corresponding chemical potential in (4.7) may take the typical form of a mixing law including the diffusion within marrow and bone,

$$L(\phi) = \frac{h(\phi) D_B}{k_B} + \frac{(1 - h(\phi)) D_M}{k_M},$$

wherein the following simple quadratic interpolation function is chosen as [61, 65]

$$h(\phi) = \phi^2 (3 - 2\phi).$$

The coefficients D_M and D_B represent the diffusivities within bone or marrow, respectively, the Fick's law being recovered in both phases. These equations successively express the evolution of the irreversible mechanical strain tensor and of the phase field, the number of produced moles, and the flux of chemical species. The variables involved in the field equations are illustrated in Figure 5.

4.4 Ginzburg–Landau equation

Furthermore, the flux of chemical species $\mathbf{J}_k$ through the boundary of the control volume ∂V leading to mineralization satisfies the following balance law:

$$\dot{n}_k^{\text{exch}} := -\nabla \cdot \mathbf{J}_k. \tag{4.8}$$

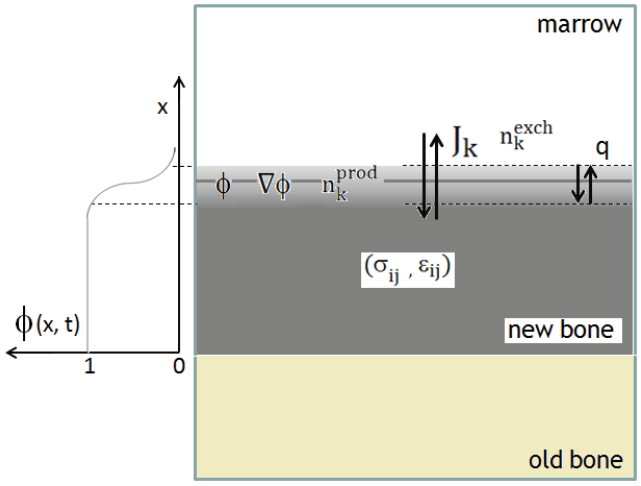

Figure 5. The three regions (old bone, new bone, and marrow) and the variables involved in the remodeling process. The phase field spatial distribution $\phi(x, t)$ is plotted.

Combining the balance equations (3.1) and (3.3) with the state equations (4.2) and (4.3) delivers the so-called Ginzburg–Landau equation governing the spatio-temporal evolution of the phase field

$$\nabla \cdot \frac{\partial \Psi}{\partial \nabla \phi} - \left(\frac{\partial \Psi}{\partial \phi} \right) = -\pi_{\phi}^{\text{diss}}. \tag{4.9}$$

The source term on the right-hand side has been defined in (4.3). The balance laws of forces and microforces, the state laws, and the kinetic equations constitute the complete set of equations one has to solve in order to describe the formation of new bone through the evolution of the interface between apposed bone and marrow.

5 Mechanical aspects

Adopting a small strain framework (the peak strains in bone is about 0.3% [28]), one may consider the usual additive decomposition of the total strain rate and the partition of the irreversible strains into strains due to mechanical and to chemical sources of dissipation:

$$\dot{\boldsymbol{\epsilon}}^{\text{irr}} = \dot{\boldsymbol{\epsilon}}^{\text{irr}}_{\text{mech}} + \dot{\boldsymbol{\epsilon}}^{\text{irr}}_{\text{prod}}.$$

The occurrence of an irreversible mechanical strain can be explained as follows: the network of osteocytes detects microcracks and local damage, which naturally involves high local strains in the vicinity of zones of ultimate strength, which in turn entails that the material locally deforms plastically. The elastic strain rate is then computed as the difference

$$\dot{\boldsymbol{\epsilon}}^{e} = \dot{\boldsymbol{\epsilon}} - \dot{\boldsymbol{\epsilon}}^{\text{irr}} = \mathbf{S} : \dot{\boldsymbol{\sigma}}.$$

Meanwhile, we can make some additional assumptions. First, we assume that the irreversible strain rate linked to the production of hydrostatic k-species is an isotropic tensor linearly depending on the rate of produced species, viz.

$$\dot{\boldsymbol{\epsilon}}^{\text{irr}}_{\text{prod}} = \gamma \dot{n}_k^{\text{prod}} \mathbf{I},$$

where $\mathbf{I}$ represents the identity tensor.

Furthermore, the production of k-species is directly correlated to the change of the order parameter reflecting the formation of new bone,

$$\dot{n}_k^{\text{prod}} = a\dot{\phi}.$$

These two assumptions lead to the following relationship:

$$\dot{\boldsymbol{\epsilon}}^{\text{irr}}_{\text{prod}} = a\gamma\dot{\phi}\mathbf{I}.$$

This leads to the following expression of the elastic strain rate:

$$\dot{\boldsymbol{\epsilon}}^{e} = \dot{\boldsymbol{\epsilon}} - a\gamma\dot{\phi}\mathbf{I} - \frac{\partial f}{\partial \boldsymbol{\sigma}}.$$

The free energy, taking into account the chemical and mechanical contributions, is expressed as

$$\Psi(\phi, \nabla\phi, \epsilon^e, n_k^{\text{exch}}, T) = \Psi_{\text{mech}}(\epsilon^e, \phi, T) + \Psi_{\text{chem}}(n_k^{\text{exch}}, \phi, \nabla\phi), \tag{5.1}$$

with the mechanical and chemical contributions therein, terms $\Psi_{\text{mech}}(\epsilon^e, \phi, T)$ and $\Psi_{\text{chem}}(n_k^{\text{exch}}, \phi, \nabla\phi)$, respectively.

Regarding mechanical aspects, the free energy of elastic deformations reads

$$\Psi_{\text{mech}}(\boldsymbol{\epsilon}^e, \phi, T) = \frac{1}{2}\boldsymbol{\epsilon}^e : C(\phi, T)\sigma : \boldsymbol{\epsilon}^e, \tag{5.2}$$

where $C(\phi, T)$ is the elastic stiffness tensor, a function of the order parameter ϕ, and depending upon the elastic properties of the medium by a mixture law including the interpolation function $h(\phi)$, involving the elasticity tensors C_B and C_M of new bone and marrow, respectively, viz.

$$C(\phi, T) = h(\phi)C_B + (1 - h(\phi))C_M.$$

Based on [61, 65–67], we adopt a chemical free energy potential of the form

$$\Psi_{\text{chem}}(n_k^{\text{exch}}, \phi, \nabla\phi) = h(\phi)\Psi_B(n_k^{\text{exch}}) + [1 - h(\phi)]\Psi_M(n_k^{\text{exch}}) + W\phi^2(1 - \phi)^2 + \frac{\alpha}{2}\nabla\phi \cdot \nabla\phi. \tag{5.3}$$

Here, the scalar parameters W and α control the diffuse interfaces behavior. Given a chemical free energy of the type "$W\phi^2(1 - \phi)^2 + \frac{\alpha}{2}\nabla\phi \cdot \nabla\phi$" and a planar interface at equilibrium, the diffuse interface width can be estimated as $\delta \cong 2\sqrt{2\alpha/W}$. Parameter α determines the strength of interfacial effects, described by the square of the Euclidean norm of the spatial gradient of the phase field, and leads to an interface energy $\sigma = \sqrt{\alpha W}/(3\sqrt{2})$ as a standard result [61, 65].

We shall select as in [61, 65] free energy densities of bone and marrow as quadratic forms in the number of exchanged chemical species

$$\Psi_B(n_k^{\text{exch}}) = \frac{1}{2}k_B(n_k^{\text{exch}} - n_{k0})^2 + \Psi_{B0}, \quad \Psi_M(n_k^{\text{exch}}) = \frac{1}{2}k_M(n_k^{\text{exch}} - n_{k0})^2 + \Psi_{M0}. \tag{5.4}$$

These energies are controlled by the curvature parameters k_B, k_M, and the constant n_{k0} therein represents the equilibrium value of the mole fraction of k-species, corresponding to the minimum of the free energy densities $\Psi_B(n_k^{\text{exch}})$, $\Psi_M(n_k^{\text{exch}})$.

By combining (4.9), (5.1), (5.2), (5.3), and (5.4), we obtain the spatio-temporal evolution of the phase field, governed by the parabolic equation

$$\tau_\phi\dot{\phi} = \alpha\Delta\phi + 2(1 - \phi)(2\phi - 1)W + 6\phi(1 - \phi)\Big[-\frac{1}{2}\epsilon^e : (C_B - C_M) : \epsilon^e + (\Psi_M - \Psi_B)\Big].$$

This equation is of the form $\dot{\phi} = F(\dot{\phi}, \Delta\phi)$, and it has to be completed with initial (IC) and boundary (BC) conditions of Dirichlet type, such as (Figure 5)

$$\begin{aligned} &\text{IC:} \quad \phi(x, t = 0) = \phi_0(x), \\ &\text{BC:} \quad \phi(x_{IM}, t) = 0, \quad \phi(x_{IB}, t) = 1. \end{aligned} \tag{5.5}$$

The spatio-temporal evolution of the reaction diffusion of produced or resorbed matter must also satisfy a field equation that can be obtained from (4.5), wherein (3.2), (4.4), (4.6), (4.7), (4.8), (5.1), and (5.4) are combined. One therefore obtains

$$\dot{n}_k^{\text{exch}} = \nabla\{L(\phi)\nabla[\phi^2(3 - 2\phi)(k_B - k_M)(n_k^{\text{exch}} - n_{k0}) + k_M(n_k^{\text{exch}} - n_{k0})]\},$$

with the following initial (IC) and boundary (BC) conditions:

$$\begin{aligned} &\text{IC:} \quad n_k^{\text{exch}}(x, t=0) = n_{k0}, \\ &\text{BC:} \quad n_k^{\text{exch}}(x_{I,M}, t) = n_{k,IM}^{\text{eq}}, \quad n_k^{\text{exch}}(x_{I,NB}, t) = 0. \end{aligned} \tag{5.6}$$

From a mechanical point of view, the stress and strain fields should satisfy the following set of equations:

$$\nabla \cdot \boldsymbol{\sigma} + f = 0, \quad \boldsymbol{\sigma} = (\phi C_B + (1-\phi) C_M) : \boldsymbol{\epsilon}^e, \quad \dot{\boldsymbol{\epsilon}}^e = \dot{\boldsymbol{\epsilon}} - \dot{\boldsymbol{\epsilon}}^{\text{irr}},$$
$$\dot{\boldsymbol{\epsilon}}^{\text{irr}} = \dot{\boldsymbol{\epsilon}}_{\text{mech}}^{\text{irr}} + \dot{\boldsymbol{\epsilon}}_{\text{prod}}^{\text{irr}}, \quad \dot{\boldsymbol{\epsilon}}_{\text{prod}}^{\text{irr}} = \gamma \dot{n}_k^{\text{prod}} \mathbf{I}, \quad \dot{\boldsymbol{\epsilon}}_{\text{mech}}^{\text{irr}} = \dot{\lambda} \frac{\partial f}{\partial \boldsymbol{\sigma}}$$

supplemented by initial and boundary conditions, as will be illustrated in the 1D example, described in Section 7.

The network of osteocytes detects microcracks and local damage, which naturally involves high local strains in the vicinity of zones of ultimate strength, which in turn entails that the material locally deforms plastically.

The irreversible mechanical strain associated to the development of the plastic zone is computed from the yield function corresponding to a Von Mises yield criterion,

$$\bar{\sigma} = \sigma_0 + \frac{\bar{\epsilon}^p}{\phi'(\bar{\sigma})},$$

with $\bar{\sigma}$ as the effective Von Mises stress and $\phi'(\bar{\sigma})$ as the (here constant) slope of the $\bar{\epsilon}^p(\bar{\sigma})$ relation. The equivalent cumulated plastic strain $\bar{\epsilon}^p$ is given by the Prandtl–Reusss flow rule:

$$\dot{\boldsymbol{\epsilon}}_{\text{mech}}^{\text{irr}} = \frac{3}{2} \phi'(\bar{\sigma}) \frac{\dot{\bar{\sigma}}}{\bar{\sigma}} \dot{\mathbf{S}},$$

with the deviatoric stress tensor $\mathbf{S} := \boldsymbol{\sigma} - \frac{1}{3}\,\text{Tr}(\boldsymbol{\sigma})\mathbf{I}$ and its rate $\dot{\mathbf{S}}$.

6 Connection between cell activity and bone production

Osteocytes are cells that form an interconnecting network in the bone tissue and differentiate into osteoblasts. The location and propagation of information signaling the mechanical damage and stress concentrations take place through this network. Osteoclasts are derived from the differentiation of stem cells in the bone marrow and can live for about 10 days. They resorb mineralized bone tissue while moving on the surface of the bone matrix. A key stimulator for osteoclast differentiation and activation is a molecule called RANK. Osteoblasts are also differentiated from stem cells in the bone marrow and express the RANKL messenger molecule and its decay receptor OPG (osteoprotegerin). Once osteoclasts have resorbed bone, they recruit osteoblasts, which fulfill the previously resorbed cavity to form osteoid, the organic part of the bone tissue. The bone formation takes about 10 times longer than resorption, and the final phase corresponds to the mineralization of the matrix. Then, osteoblasts differentiate into osteocytes after 2 weeks and are inserted into the newly formed bone or they die.

Coordination of osteoclasts, osteoblasts, and osteocytes in a BMU (Figure 6) is performed through a complex exchange of information that passes through autocrine signaling pathways (between cells of the same type) and paracrine (between cells of different types) and various couplings. Among the messengers involved, RANKL and OPG play a critical role both in the physiological bone remodeling and in the development of diseases. RANKL has a stimulating effect on the differentiation of osteoclast precursors and subsequent activation of mature osteoclasts in the resorption of the active cells. The OPG molecule produced by mature osteoblasts acts as a decay receptor for RANKL, inhibiting the RANK-RANKL bond formation and thereby the stimulation of osteoclasts. A high ratio of RANKL/OPG promotes the bone resorption phenomenon, whereas a low ratio leads to a decrease in osteoclast activity. Meanwhile, it seems that canalicular fluid flow is responsible for osteoclast activity and their ability to move in the BMU.

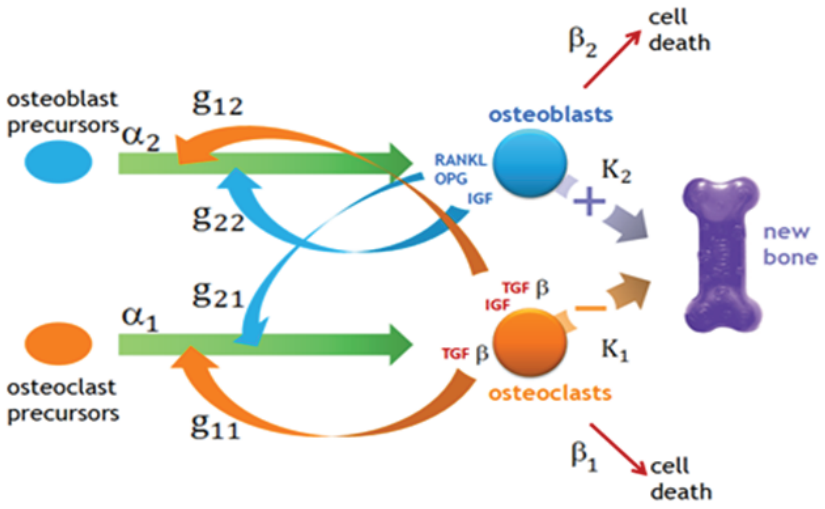

Figure 6. Dynamic system illustrating cell activity and the different interactions leading to the formation of new bone or bone resorption [51].

6.1 Production of bone mass

As emphasized in [16], predictive models of bone remodeling generally ignore the coupled activity of the specialized cells (osteoclasts, osteoblasts, and osteocytes), which combines with the mechanical response of bone. The cell activity involves many interactions between families of cells and their precursors, as illustrated in Figure 6. We shall consider here the well-known model of Komarova et al. [51], which synthetically describes these phenomena. Here, we remember that the osteocytes sense the mechanical stimulus and transmit the information to the other cells located in their vicinity. The scheme adopted by previous authors describes the effects of osteoblasts and osteoclasts precursors on the mature cells and includes the feedback effect and the interaction between osteoblasts producing material and osteoclasts responsible for resorption. The various produced biochemical factors (RANKL, OPG, IGF, and IGF TGF β) are at the origin of these effects. The corresponding dynamic system of equations is given as

$$\dot{n}_{\mathrm{oc}} = \alpha_1 n_{\mathrm{oc}}^{g_{11}} n_{\mathrm{ob}}^{g_{21}} - \beta_1 n_{\mathrm{oc}}, \quad \dot{n}_{\mathrm{ob}} = \alpha_2 n_{\mathrm{oc}}^{g_{12}} n_{\mathrm{ob}}^{g_{22}} - \beta_2 n_{\mathrm{ob}},$$

where $n_{\mathrm{ob}}(t)$ and $n_{\mathrm{oc}}(t)$ represent the total numbers of osteoblasts and osteoclasts, respectively (they reach equilibrium values denoted as $n_{\mathrm{oc}}^{\mathrm{eq}}$ and n_{ob}^{q}, and the exponents g_{11}, g_{12}, g_{21}, and g_{22} transduce the transduction phase by the osteocytes, which sense mechanical signals and activate osteoblasts and osteoclasts in response. Previous system describes the temporal changes of the osteoclasts and osteoblasts populations including the autocrine and paracrine regulations between both populations. The eight parameters of this non-linear system represent the mutual effects, interaction, and feedback among the cell populations. Thus, parameters α_1 and α_2 reflect the effect of precursors of osteoclasts and osteoblasts on the osteoclasts and osteoblasts proliferation; in contrast, parameters β_1, β_2 are the speed of the cell degradation process. It is now possible to establish a link between the antagonist cell activity of osteoclasts and osteoblasts. To do this, let us consider only the active cells N_1 and N_2 that represent a fraction of the full populations ($n_1 = n_{\mathrm{oc}}$, $n_2 = n_{\mathrm{ob}}$),

$$N_i = H(n_i - \bar{n}_i),$$

where $H(x) = \frac{x+|x|}{2}$ is the usual ramp function and $\bar{n}_i$ is the number of cells i at steady state. The formation of new bone is described by the mass production term $\dot{m}$ which satisfies the equation

$$\frac{dm}{dt} = -K_1 N_1 + K_2 N_2 = \sum_k \dot{n}_k^{\mathrm{prod}} M_k = \sum_k (\dot{n}_k^{\mathrm{prod}} + \dot{n}_k^{\mathrm{exch}}) M_k = V \frac{d\rho}{dt},$$

where K_1 and K_2 are the normalized cell activities in terms of mass production.

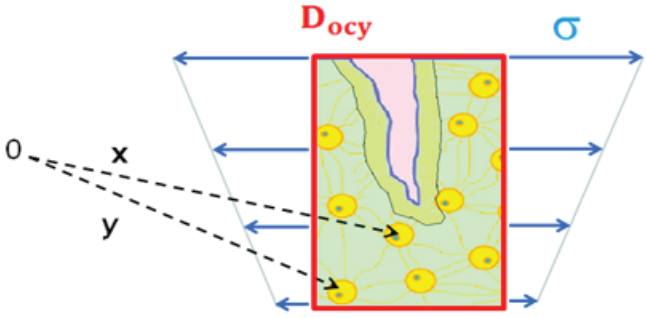

Figure 7. Perception of the mechanical stimulus by the network of osteocytes.

6.2 Equilibrium solutions for the cell populations

Given the dynamic system of the model expressed in [51] we examine the different solutions, especially those leading to equilibrium [51]. The equilibrium points ($\dot{n}_{oc}^{eq} = \dot{n}_{ob}^{eq} = 0$) corresponding to the stability of the cell populations are easily computed as

$$n_{oc}^{eq} = \left(\frac{\beta_1}{\alpha_1}\right)^{\frac{1-g_{22}}{\Gamma}} \left(\frac{\beta_2}{\alpha_2}\right)^{\frac{g_{21}}{\Gamma}}, \quad n_{ob}^{eq} = \left(\frac{\beta_1}{\alpha_1}\right)^{\frac{g_{12}}{\Gamma}} \left(\frac{\beta_2}{\alpha_2}\right)^{\frac{1-g_{11}}{\Gamma}},$$

with $\Gamma := g_{12}g_{21} - (1 - g_{11})(1 - g_{22})$.

Depending on the sign of $\Phi = \beta_1(g_{11} - 1) + \beta_2(g_{22} - 1)$, the model predicts different types of dynamic behavior: for $\Phi = 0$, one obtains a periodic solution, the case $\Phi < 0$ leads to damped oscillations converging to n_{oc}^{eq} and n_{ob}^{eq}, and the last situation $\Phi > 0$ to unstable oscillations. The computation of the solution for a 1D problem will be done in Section 7.

6.3 Cell activity in relation to the mechanical stimulus

As we noted above, and following the model of Bonfoh et al. [58], the sensing activity of osteocytes may be connected to mechanical stimuli through the deformation energy of the bone at the vicinity of the region of high stress concentration such as microcracks. Thus, one may assume that

$$g_{ij} = g_{ij}(\Delta Y),$$

with the following mechanical signal obtained as a volume integral over a characteristic zone D_{ocy} including a crack (Figure 7) and submitted to a stress field corresponding to a combined tension and bending (i.e. corresponding the mode 1 of crack opening),

$$\Delta Y(x) = \int_{D_{ocy}} dV f(x,y)\left(\frac{\omega(y)}{\rho(y)} - w_0\right) = \left(\int_{D_{ocy}} dV f(x,y)\frac{\omega(y)}{\rho(y)}\right) - S_0$$

including the specific strain energy $\frac{\omega(y)}{\rho}$, with $\omega(y) = \frac{1}{2}\sigma(y) : \epsilon(y)$.

The spatial influence function may be defined as the following fading exponential:

$$f(x,y) = \begin{cases} 0 & \text{if } d > R_{OC}, \\ e^{-d(x,y)/R_{OC}} & \text{if } d \le R_{OC}, \end{cases}$$

in which $d(x,y) = |x - y|$ is the distance between the considered osteocytes and pre-osteoclasts or pre-osteoblasts. According to [58], it is estimated that no signal will be received from the outside of this zone of influence. Finally, the signal received by osteoclasts and osteoblasts influences the autocrine and paracrine factors through the exponents g_{ij}.

The bending load applied to a trabeculum (Figure 8) causes a tensile stress on one side and a compressive stress on the opposite side. This generates pressure gradients driving the fluid flow through the canaliculae and across the osteocytes from regions in compression to regions in tension, providing the nutrients.

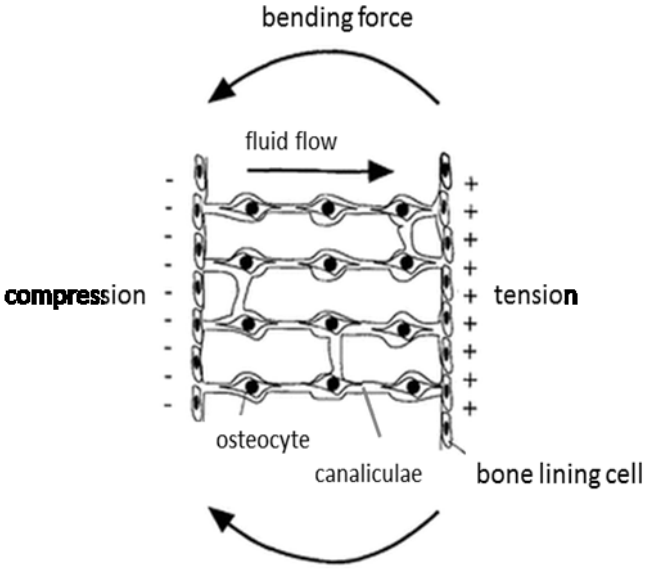

Figure 8. Schematic representation of a trabeculum under bending load [68].

7 One-dimensional example

We analyze bone formation or resorption within a rectangular domain (Figure 9) corresponding to a biological situation shown in Figure 8, relying on the field equations written in previous sections.

7.1 Boundary value problem

Accounting for the selected form of the stress field and assuming that the component $\sigma_{xx} = -p$ is uniform (corresponding to the boundary condition at the horizontal edge $x = h_m(t)$), mechanical equilibrium leads to the following stress field:

$$\boldsymbol{\sigma} = \sigma_{xx}(y)\mathbf{e}_x \otimes \mathbf{e}_x + \sigma_{yy}(x)\mathbf{e}_y \otimes \mathbf{e}_y = -p\mathbf{e}_x \otimes \mathbf{e}_x + (\sigma_m + ax)\mathbf{e}_y \otimes \mathbf{e}_y. \tag{7.1}$$

Consideration of the lateral boundary condition along the vertical edge with consideration of the chosen form of the stress component $\sigma_{yy}(x)$ corresponding to a combination of tension and bending leads to (we consider a domain with unity thickness)

$$\int_0^{h_m(t)} \sigma_{yy}(x,t)dx = F \quad \Rightarrow \quad \sigma_m h_m(t) + \frac{a(t)}{2} h_m(t)^2 = F, \tag{7.2}$$

which provides a relation between the stress gradient parameter $a(t)$ and the domain height, $h_m(t)$, delimiting the border between bone formation region and marrow; previous relation clearly means that the stress gradient controls the speed of remodeling through the size of the grown domain. The stress field in (7.1) is accordingly equilibrated when conditions (7.3) below are satisfied. The plastic strain tensor may be evaluated after straightforward computations using the following well-known flow rule:

$$d\boldsymbol{\epsilon}^p = d\lambda \frac{\partial g(\boldsymbol{\sigma})}{\partial \boldsymbol{\sigma}},$$

where λ and $g(\boldsymbol{\sigma})$ represent the plastic multiplier and the stress surface, respectively.

The domain is subjected to an applied stress normal to the crack opening (oriented along y) and presenting a gradient along the x direction, so that

$$\boldsymbol{\sigma}^{\text{ext}}(x) = \sigma_{yy}(x)\mathbf{e}_y \otimes \mathbf{e}_y, \quad \sigma_{yy}(x) = \sigma_m + ax, \tag{7.3}$$

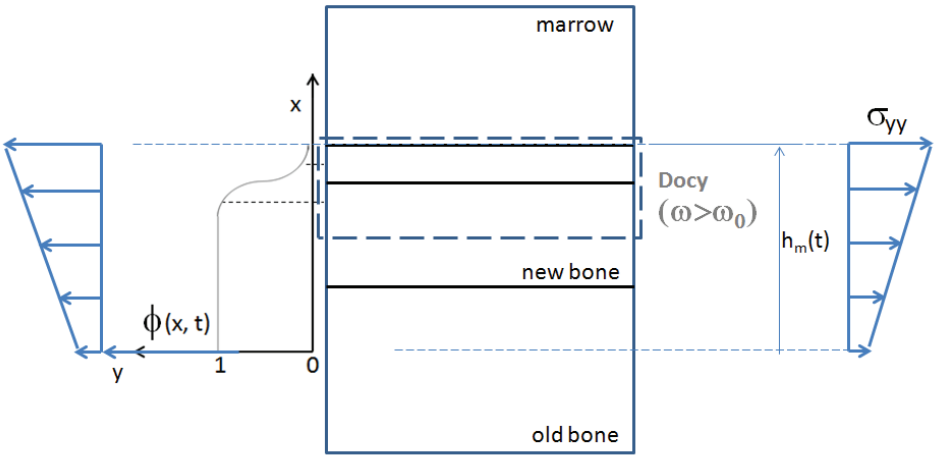

Figure 9. Domain with formation of new bone and network of osteocytes (Docy).

with σ_m as the stress at the bottom edge ($x = 0$) and the constant a controlling the stress gradient intensity. We presently assume the stress field to depend only on the x coordinate (the domain is thin enough in the y direction such that the stress and strain gradients in this direction can be neglected). The mechanical boundary conditions are the following (Figure 7):

$$\mathbf{u}(x = 0, t) = \mathbf{0}, \quad \mathbf{t}\left(x = \pm\frac{1}{2}, t\right) = (\sigma_m + ax)\mathbf{e}_x, \quad \int_{S_h} \mathbf{t}(x, t)dS = F\mathbf{e}_x. \tag{7.4}$$

The first BC expresses the clamped bottom edge, the second the applied traction along the domain vertical edges, and the third the applied constant vertical force F on the top edge.

We aim at computing both the propagation along x of the diffuse interface within which mineralization takes place. Neglecting the strain energy contribution of the marrow (the bulk modulus of the marrow phase is a few megapascals), the elastic contribution depends on the relative elastic energy, quantity

$$\frac{1}{2}\boldsymbol{\epsilon}^e : (C_B - C_M) : \boldsymbol{\epsilon}^e \approx \frac{1}{2}\boldsymbol{\epsilon}^e : C_B : \boldsymbol{\epsilon}^e \approx \frac{1}{2}\boldsymbol{\sigma} : C_B^{-1} : \boldsymbol{\sigma} = \frac{1}{2}\sigma_{xx}^2\{C_B^{-1}\}_{xxxx} + \frac{1}{2}\sigma_{yy}^2\{C_B^{-1}\}_{yyyy} \tag{7.5}$$

with the compliance coefficients therein given versus the homogenized moduli in x and y directions as

$$\{C_B^{-1}\}_{xxxx} = \frac{1}{E_x^*}, \quad \{C_B^{-1}\}_{yyyy} = \frac{1}{E_y^*}. \tag{7.6}$$

The stress components σ_{xx}, σ_{yy} correspond to the applied mechanical loading; the stress component σ_{yy} is varied by changing the slope $a(t)$; this in turn modifies the height of the interface between bone and marrow, the variable $h_m(t)$, obtained as the solution of (7.2).

Bone is considered as an orthotropic effective material, with effective properties given from the homogenization of an hexagonal prototype microstructure, adopting a relative density $\rho^*/\rho_s = 0.19$, with $\rho_s = 2000\ \mathrm{kg/m^3}$, and [64]

$$E_x^* = 0.014E_s, \quad E_y^* = 0.067E_s.$$

The bulk modulus of the trabeculae is taken as $E_s = 12$ GPa [69]. The characteristic time τ_ϕ is computed based on the relation

$$\tau_\phi = \frac{L^2}{D}$$

with L as a characteristic diffusion length, itself evaluated from the average velocity of apposition of mineral,

$$\bar{V} := \frac{L}{\tau_\phi} \quad \Rightarrow \quad \tau_\phi = \frac{D}{\bar{V}^2} \approx 8.64 \times 10^6\ \mathrm{s\,J\,m^{-3}}$$

Parameter	Value
Loading data	$p := 10^6$ Pa, $F = 10^3$ N, $\sigma_m := 1$ MPa
Diffusion coefficient	$D_m = 10^{-12}$ m^2 s^{-1}
Relaxation time for mineral apposition	$\tau_\phi = 8.64 \times 10^6$ s J m^{-3}
Interfacial free energy penalty parameter	$W = 10^3$ J m^{-3}
Curvatures of the chemical free energy	$k_B = 10^5$ J, $k_M = k_B/100$
Coefficient α in Ginzburg–Landau equation	$\alpha = 8.64 \times 10^{-6}$ J m^{-1}
Bone effective orthotropic moduli in x and y directions	$E_{xx} = 0.17$ GPa, $E_{yy} = 0.8$ GPa

Table 1. Value of the model parameters.

representing a duration of 100 days. This entails the determination of the coefficient α in the Ginzburg–Landau equation

$$\frac{\alpha}{\tau_\phi} = D = 10^{-12}\ \mathrm{m^2 s^{-1}} \quad \Rightarrow \quad \alpha = D\tau_\phi \approx 8.64 \times 10^{-6}\ \mathrm{J\,m^{-1}}.$$

It is realistic to neglect diffusion in bone, so that the influence coefficient for diffusion simplifies to the following function of the phase field variable:

$$L(\phi) = [1 - h(\phi)]\frac{D_M}{k_M}.$$

The curvature coefficient is much smaller in the formed bone compared to marrow; thus, we select $k_M = k_B/100$. The selected model parameters are summarized in Table 1.

7.2 Algorithm for the resolution of the system of PDEs

One shall solve the following system of two coupled PDEs for the phase field $\phi(x, t)$ and chemical concentrations $n_k^{\mathrm{exch}}(x, t)$:

$$\begin{cases} \tau_\phi \dot{\phi} = \alpha\Delta\phi + 2\phi(1-\phi)(2\phi-1)W + 6\phi(1-\phi)\Big[-\frac{1}{2}\epsilon^e : (C_B - C_M) : \epsilon^e + (\Psi_M - \Psi_B)\Big], \\ \Psi_B(n_k^{\mathrm{exch}}) = \frac{1}{2}k_B(n_k^{\mathrm{exch}} - n_{k0})^2 + \Psi_{B0}, \\ \Psi_M(n_k^{\mathrm{exch}}) = \frac{1}{2}k_M(n_k^{\mathrm{exch}} - n_{k0})^2 + \Psi_{M0}, \\ \dot{n}_k^{\mathrm{exch}} = \nabla\{L(\phi)\nabla[\phi^2(3-2\phi)(k_B - k_M)(n_k^{\mathrm{exch}} - n_{k0}) + k_M(n_k^{\mathrm{exch}} - n_{k0})]\}, \\ L(\phi) = [1 - \phi^2(3-2\phi)]\frac{D_M}{k_M}. \end{cases}$$

Due to the quite slow remodeling process in comparison to the return to equilibrium of the mechanical response, one can consider a succession of quasistatic problems, thus neglecting the time derivatives in previous equations. After normalization of the spatial variable x by the thickness parameter h_n (one adopts the non-dimensional spatial variable $\tilde{x} := x/h_n$) and simplification of the second PDE by the constant factor D_M/k_M (intermediate quantities are computed in Appendix A), one then obtains the following static boundary value problem in normalized form:

$$\frac{\alpha}{h_n^2}\partial^2_{\tilde{x}\tilde{x}}\phi + 2\phi(1-\phi)(2\phi-1)W + 6\phi(1-\phi)\Big[-\frac{1}{2}\epsilon^e : (C_B - C_M) : \epsilon^e + (\Psi_M - \Psi_B)\Big] = 0,$$
$$\partial_{\tilde{x}}\Big\{\Big([1-\phi^2(3-2\phi)]\frac{D_M}{k_M}\Big)\partial_{\tilde{x}}[\phi^2(3-2\phi)(k_B - k_M)(n_k^{\mathrm{exch}} - n_{k0}) + k_M(n_k^{\mathrm{exch}} - n_{k0})]\Big\} = 0,$$

with the new spatial dependencies $\phi(x) = \tilde{\phi}(\tilde{x})$, $n(x) = \tilde{n}(\tilde{x})$. The second equation yields a first integral

$$\Big([1-\phi^2(3-2\phi)]\frac{D_M}{k_M}\Big)\partial_{\tilde{x}}[\phi^2(3-2\phi)(k_B - k_M)(n_k^{\mathrm{exch}} - n_{k0}) + k_M(n_k^{\mathrm{exch}} - n_{k0})] = Cte.$$

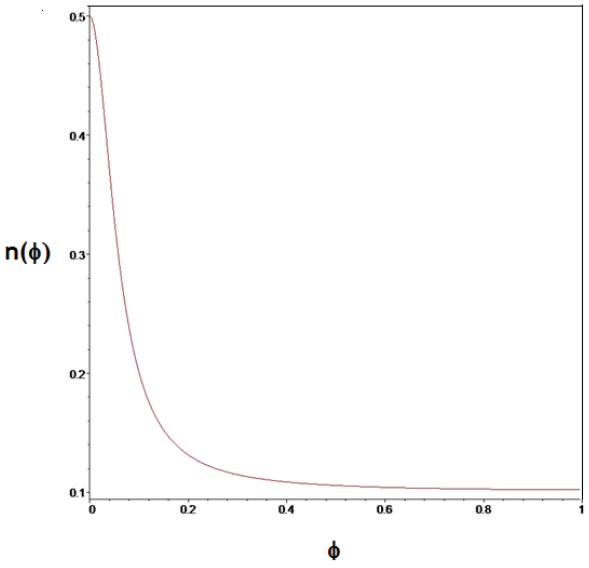

Figure 10. Evolution of the chemical concentration of the mineral phase versus the phase field. $n_{k0} = 0.1$, $n_{kM}^{\infty} = 0.5$.

The constant therein vanishes considering the value $\phi = 1$ of the phase field in the bone phase; this yields

$$\{\phi^2(3-2\phi)(k_B - k_M) + k_M\}(n_k^{\text{exch}} - n_{k0}) = Cte$$

with the constant determined from the boundary condition in the phase in which the phase field vanishes, viz. $n_k^{\text{exch}} \equiv n_{kM}^{\infty}$ representing the mineral concentration in the marrow phase, in the spatial domain characterized as the epigraph of the phase field $\{x/\phi(x,t) \leq \phi_{\min} = 0.05\}$. Previous equality delivers the following expression of the molar concentration versus the phase field, as

$$n_k^{\text{exch}}(x) - n_{k0} = \frac{n_{kM}^{\infty} - n_{k0}}{\phi^2(3-2\phi)(k_B/k_M - 1) + 1}.$$

This in turn delivers the following ODE for the phase field:

$$\begin{aligned}
&\frac{\alpha}{h_n^2}\partial^2_{\tilde{x}\tilde{x}}\phi - \frac{6\phi(1-\phi)}{2}\epsilon^e : (C_B - C_M) : \epsilon^e \\
&\quad + 6\phi(1-\phi)\left\{\frac{1}{2}(k_M - k_B)\left[\frac{(n_{kM}^{\infty} - n_{k0})}{\phi^2(3-2\phi)(k_B/k_M - 1) + 1}\right]^2 + \Psi_{M0} - \Psi_{B0}\right\} \\
&\quad + 2\phi(1-\phi)(2\phi - 1)W = 0.
\end{aligned}$$

The following boundary conditions are adopted in the physical domain:

$$\phi(x_{IM}, t) = 0.05, \quad \phi(x_{IB}, t = 0) = 0.95, \quad n_k^{\text{exch}}(x_{IM}, t = 0) = 0.95, \quad n_k^{\text{exch}}(x_{IB}, t = 0) = 0.05.$$

The evolution of the molar concentration versus the phase field variable is represented in Figure 10, selecting the following values for the equilibrium and far field marrow concentrations, $n_{k0} = 0.1$, $n_{kM}^{\infty} = 0.5$; the concentration of mineral decreases rapidly with the degree of mineralization up to saturation.

We have denoted the position of the new bone/marrow and old bone/new bone interfaces by $x_{IB} \approx 0$ and $x_{IM}(t)$, respectively; the second variable $x_{IM}(t)$ is changing with time due to remodeling and has to be computed from the solution obtained at each new time increment. Denoting $\tilde{x}_{IM} = x_{IM}/h_n$, $\tilde{x}_{IB} = x_{IB}/h_n$, the counterparts of the boundary conditions expressed in the non-dimensional spatial variables are

$$\tilde{\phi}(\tilde{x}_{IM}, t) = 0.05, \quad \tilde{\phi}(\tilde{x}_{IB}, t = 0) = 0.95, \quad \tilde{n}_k^{\text{exch}}(\tilde{x}_{IM}, t = 0) = 0.95, \quad \tilde{n}_k^{\text{exch}}(x_{IB}, t = 0) = 0.05.$$

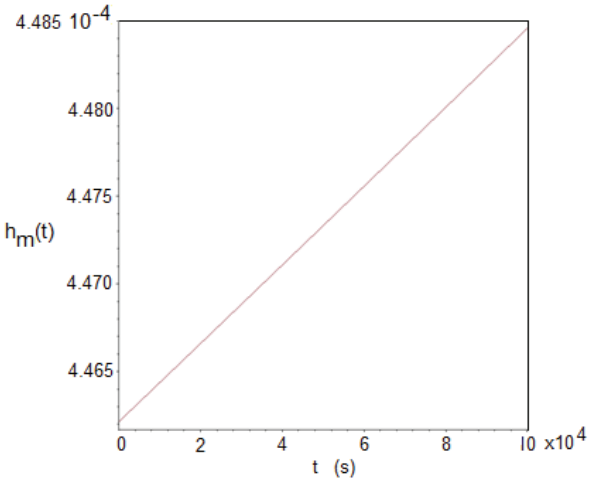

Figure 11. Evolution of the interface height versus time. $a(t) = a_0 + kt$ with $a_0 = 10^{10}$ MPa m^{-1}, $k = -10^3$ MPa m^{-1} s^{-1}.

The interface height separating newly formed bone from marrow is obtained by solving the balance of forces, (7.4), using the form of the stress field given in (7.3):

$$h(t) = \frac{-\sigma_m + (2Fa(t) + \sigma_m^2)^{1/2}}{a(t)}.$$

The stress field varies nearly linearly versus time for the chosen slope parameter $a(t) = a_0 + kt$, as shown in Figure 11.

7.3 Effect of mechanical and chemical energies on remodeling

We aim at determining the relative influence of the mechanical and chemical energies on the remodeling process, relying on the idea that remodeling or resorption will occur according to the respective contribution of each type of energy contribution.

We first determine the reference solution (fictive) in the absence of chemical and mechanical energies, writing the set of local equations in non-dimensional form considering an density energy variation reference value of $|\delta\Psi| = k_M$ (or $|\delta\Psi| = \Psi_M^0 - \Psi_B^0$); this is achieved by defining the following reduced parameters: the reduced time $t^* = |\delta\Psi|t/\tau_\phi$; the reduced spatial variable $r^* = r/l$, with l as the characteristic length of the problem, typically the interface width; the non-dimensional gradient is defined as $\nabla^* = l\nabla$. Moreover,

$$\alpha^* = \frac{\alpha}{|\delta\Psi|l^2}, \quad \Psi_M^* = \frac{\Psi_M}{|\delta\Psi|}, \quad \Psi_B^* = \frac{\Psi_B}{|\delta\Psi|}, \quad W^* = \frac{W}{|\delta\Psi|},$$
$$C_B^* = \frac{C_B}{|\delta\Psi|}, \quad C_M^* = \frac{C_M}{|\delta\Psi|}, \quad L^*(\phi) = L(\phi)\frac{\tau_\phi}{l^2}, \quad k_B^* = \frac{k_B}{|\delta\Psi|}, \quad k_M^* = \frac{k_M}{|\delta\Psi|.}$$

Based on the introduced reduced spatial and time scales, the non-dimensional form of the local differential equations for the phase field and chemical concentration is

$$\frac{\partial\phi}{\partial t^*} = \alpha^*\Delta^* + 2\phi(1-\phi)(2\phi-1)W^* + 6\phi(1-\phi)\left[-\frac{1}{2}\epsilon^e : (C_B^* - C_M^*) : \epsilon^e + (\Psi_M^* - \Psi_B^*)\right], \tag{7.7}$$
$$\frac{\partial n_k^{\text{exch}}}{\partial t^*} = \nabla^* \cdot \{L^*(\phi)\nabla^*[\phi^2(3-2\phi)(k_B^* - k_M^*) + k_M^*](n_k^{\text{exch}} - n_{k0})\}.$$

The last two terms in the phase field parabolic equation represents contributions from mechanical and chemical energies; the equilibrium concentration n_k^{exch} is seen to depend on the elastic strain, due to the indirect coupling of elastic strains with the phase field variable. This means one cannot truly distinguish

purely chemical from purely mechanical energy in the PDE governing the phase field variable. To analyze the influence of the overall energy contribution

$$\alpha^*\Delta^*\phi + 2\phi(1-\phi)(2\phi-1)W^* + 6\phi(1-\phi)\Big[-\frac{1}{2}\epsilon^e : (C_B^* - C_M^*) : \epsilon^e + (\Psi_M^* - \Psi_B^*)\Big]$$

on the local bone remodeling process within the diffuse interface, we first take as a reference solution the phase field $\phi^*(x^*)$ satisfying the stationary PDE, termed the stability equation,

$$\frac{\partial\phi}{\partial t^*} = 0 = \alpha^*\Delta^*\phi + 2\phi(1-\phi)(2\phi-1)W^*. \tag{7.8}$$

Its solution is a hyperbolic tangent of the form

$$\phi^R(x^*) = \frac{1}{2} + \frac{1}{2}th\Big(\frac{a-x^*}{b}\Big).$$

Parameter a corresponds to the interface position for $\phi = 1/2$, and $b = \sqrt{2\alpha^*/W^*}$. This solution is stable in the sense that the phase field does not change in time locally (in the absence of chemical and mechanical energies).

The motion of the diffuse interface will lead to remodeling (respectively, resorption) if any point with a fixed spatial position will experience a local increase (respectively, decrease) in time of the phase field variable, i.e. if the time derivative $\frac{d\phi}{dt^*}$ is non-negative (respectively, negative). The sign of the last derivative is influenced by the additional chemo-mechanical energetic contribution

$$6\phi(1-\phi)\Big[-\frac{1}{2}\epsilon^e : (C_B^* - C_M^*) : \epsilon^e + [\Psi_M^*(n_k^{\text{exch}}) - \Psi_B^*(n_k^{\text{exch}})]\Big].$$

Considering the fact that $6\phi(1-\phi) > 0$ and $\frac{1}{2}\epsilon^e : (C_B^* - C_M^*) : \epsilon^e > 0$, remodeling (respectively, resorption) will take place locally when last quantity is positive (respectively, negative). Note that the chemical concentration n_k^{exch} depends on the elastic strain through the phase field variable.

To get a qualitative understanding on the behavior of our BMU model system under stress, we will first assume that the quantity $\alpha^*\Delta^*\phi + 2\phi(1-\phi)(2\phi-1)W^*$ in (7.8) is always equal to zero, thus leading to a fixed shape of the interface. This assumption is obviously only an approximation, considering the fact that ϕ is coupled with n_k^{exch} and that the additional chemo-mechanical energetic contribution will also change the shape of the interface. In any case, the interface will have in case of small perturbations a shape not far from the form given by $\phi^R(x^*)$ or at least with the same tendency. Considering this assumption, the interface motion will be determined by the sign of the quantity

$$-\frac{1}{2}\epsilon^e : (C_B^* - C_M^*) : \epsilon^e + [\Psi_M^*(n_k^{\text{exch}}) - \Psi_B^*(n_k^{\text{exch}})]$$

calculated at the position $x^* = h_m$ of the interface.

The mechanical energy (the first term in previous sum) is evaluated versus the stress as

$$\frac{1}{2}\epsilon^e : (C_B - C_M) : \epsilon^e \approx \frac{1}{2}\frac{\sigma_{xx}^2}{E_x^*} + \frac{1}{2}\frac{\sigma_{yy}^2}{E_y^*}.$$

Relying on (7.3), (7.5), and (7.6), we obtain a simple form of the stress tensor at $x^* = h_m$ as follows:

$$\sigma_{xx} = -p, \quad \sigma_{yy}(h_m(t)) = \frac{2F}{h_m(t)} - \sigma_m.$$

This leads to a mechanical term of the form

$$\frac{1}{2}\epsilon^e : (C_B - C_M) : \epsilon^e \approx \frac{1}{2}\frac{p^2}{E_x^*} + \frac{1}{2E_y^*}\Big(\frac{2F}{h_m(t)} - \sigma_m\Big)^2,$$

where $h_m(t)$ is the interface position at given time t and F is an external force applied to the BMU model system. In Figure 12, the mechanical term is plotted as a function of the ratio $2F/h_m(t)$, which leads to

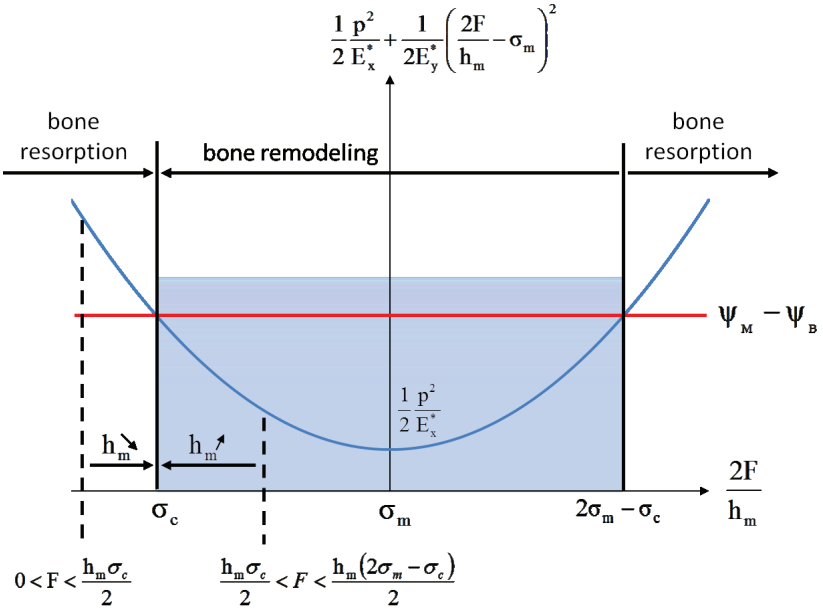

Figure 12. Plot of the mechanical contribution as a function of $2F/h_m$ for a given interface at position h_m under an applied force F, compared to the chemical term $\Psi_M - \Psi_B$, considered here as a constant (solid horizontal red line).

a simple parabolic shape centered on the residual stress σ_m and which is compared to the chemical term $[\Psi_M - \Psi_B]$, represented as a constant (horizontal plain line in Figure 12).

According to Figure 12, the following comparison rules hold between both previous energy contributions:

$$\frac{1}{2}\frac{p^2}{E_x^*} + \frac{1}{2E_y^*}\left(\frac{2F}{h_m} - \sigma_m\right)^2 \begin{cases} < \Psi_M - \Psi_B & \text{if } \frac{2F}{h_m} \in]\sigma_c, 2\sigma_m - \sigma_c], \\ > \Psi_M - \Psi_B & \text{if } \frac{2F}{h_m} < \sigma_c \text{ or } \frac{2F}{h_m} > 2\sigma_m - \sigma_c. \end{cases} \tag{7.9}$$

In the first case in (7.9), the derivative $\frac{d\phi}{dt^*}$ takes positive values, which leads to an increase in ϕ values at the interface, i.e. bone remodeling. In the second case in (7.9), the derivative $\frac{d\phi}{dt^*}$ takes negative values, which leads to a decrease in ϕ values at the interface, i.e. bone resorption.

Several conditions can be deduced from these inequalities, in line with Figure 12. First, force F and residual stress σ_m should already be present (with non-vanishing values), which makes sense from a biological viewpoint. Second, considering an interface at a given fixed position h_m, the interface profile should verify the condition

$$\frac{1}{2}\frac{p^2}{E_x^*} + \frac{1}{2E_y^*}\left(\frac{2F}{h_m} - \sigma_m\right)^2 = \Psi_M - \Psi_B$$

at position $x = h_m$. This implies that the quantity $\Psi_M - \Psi_B$ should be positive at the interface for bone remodeling to take place.

For instance, a fixed interface at $x = h_m^0$ is obtained for

$$\frac{2F^0}{h_m^0} = \sigma_c \quad \text{or} \quad \frac{2F^0}{h_m^0} = 2\sigma_m - \sigma_c.$$

Case $2F^0/h_m^0 = \sigma_c$: Any applied force $F > F^0$ increases the quantity $2F/h_m^0$, which then falls into the bone remodeling domain as long as $2F/h_m^0 \in]\sigma_c, 2\sigma_m - \sigma_c]$. Remodeling then increases the interface height h_m ($> h_m^0$), which leads to a decrease in quantity $2F/h_m$ until $2F/h_m = \sigma_c$ for which a new stable position of the interface is reached at position $x = h_m > h_m^0$. On the contrary, any applied force $F < F^0$ decreases the quantity $2F/h_m^0$, which falls into the bone resorption domain. Resorption entails a decrease in interface height h_m ($< h_m^0$), which leads to an increase in quantity $2F/h_m$ until $2F/h_m = \sigma_c$, for which a new stable position of the interface is reached at $x = h_m < h_m^0$.

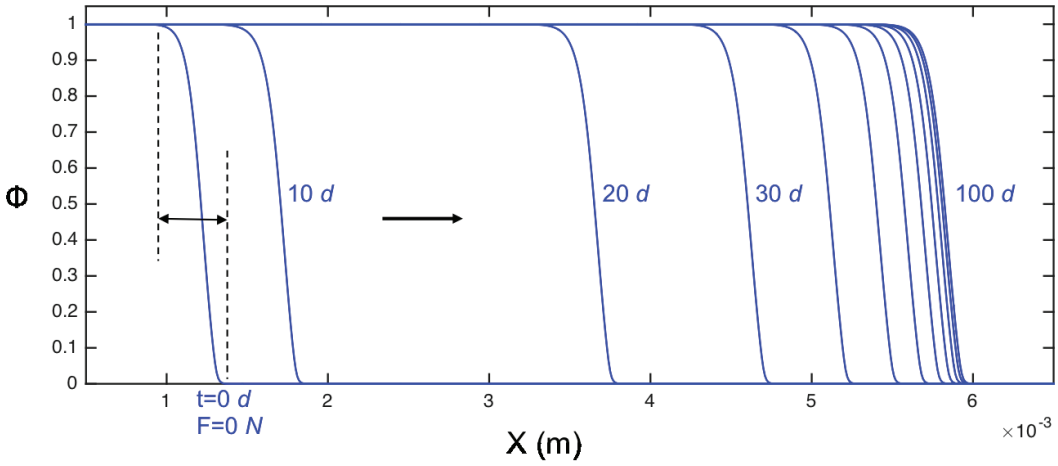

Figure 13. Evolution versus time (in days) of the spatial distribution of the phase field solved in one dimension (see (7.7)) with an external force $F = 1000$ N, starting from an equilibrium configuration at $t = 0$ with no external force.

In this first case, increasing progressively the force F leads to bone remodeling, whereas decreasing the force F leads to bone resorption.

Case $2F^0/h_m^0 = 2\sigma_m - \sigma_c$: Any applied force $F > F^0$ increases quantity $2F/h_m^0$, which then falls into the bone resorption domain. Resorption leads to a decrease in h_m ($< h_m^0$), which leads to an increase in quantity $2F/h_m$ until complete bone resorption. On the opposite, any applied force $F < F^0$ decreases quantity $2F/h_m^0$, which then falls into the bone remodeling domain. A remodeling behavior entails an increase in interface height h_m ($> h_m^0$), which leads to a decrease in quantity $2F/h_m$ until $2F/h_m = \sigma_c$, where a new stable position of the interface is reached at $x = h_m > h_m^0$.

Case $2F^0/h_m^0 = \sigma_c$ seems to be closer to reality: in that case, the position of the interface can be calculated as a function of F; in this case, additional conditions to be satisfied by the quantity $\Psi_M - \Psi_B$ can be also deduced (see Appendix B):

$$h_m = \frac{2F}{\sigma_m - \sqrt{2E_y^*}\sqrt{(\Psi_M^* - \Psi_B^*) - p^2/(2E_x^*)}} \quad \text{with } \frac{p^2}{2E_x^*} < \Psi_M - \Psi_B < \frac{\sigma_m^2}{2E_y^*} + \frac{p^2}{2E_x^*}.$$

It is important to note that increasing the force in time much faster than the kinetics of bone remodeling will lead to a metastable situation because the BMU does not have enough time to adjust to the imposed effort.

Figure 12 shows a simple 1D example of bone remodeling under stress. Note that the interface remains localized (it does not thicken); thickening occurs for the bone phase. The spatial distribution of the phase field (Figure 13) generates, according to Figure 10, a similar distribution of the fraction of the mineral phase. The application of a resultant $F = 1000$ N moves the bone/marrow interface, up to a new equilibrium position is reached (after about 100 days), as shown in Figure 13.

7.4 Evolution versus time of the number of osteoblasts and osteoclasts

Based on the solution of the field equations for the phase field and chemical concentrations at the continuum level, one shall next solve at the cellular level the dynamic system for the population of osteoclasts and osteoblasts given in Section 6.

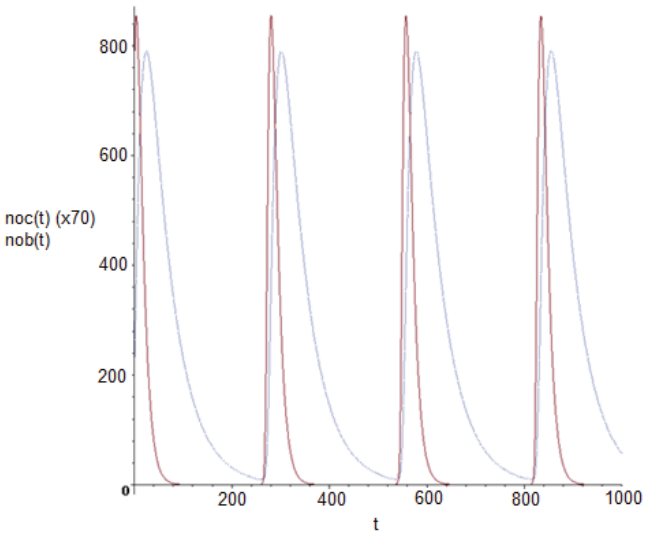

Figure 14. Stable regulated oscillatory changes in bone cell populations and bone mass: red line, osteoclasts (×70); blue line, osteoblasts. Calculations are performed with the following parameters: $\alpha_1 = 3$, $\alpha_2 = 4$, $\beta_1 = 0.2$, $\beta_2 = 0.02$, $g_{11} = 1.1$, $g_{12} = 1$, $g_{21} = -0.5$, $g_{22} = 0$. Initial number of cells: 11 osteoclasts and 212 osteoblasts [51].

We shall select in view of numerical illustrations the following parameters:

$$g_{11} = 0.5, \quad g_{22} = 0, \quad g_{12} = 1, \quad g_{21} = -0.5$$
$$w_0 = 0.002\ \text{J/g}, \quad \rho_L = 1.2\ \text{g/cm}^3, \quad R_{\text{OC}} = 100\ \mu\text{g},$$
$$g_{11} = A_1 + B_1 e^{-\gamma_1 \Delta Y}, \quad g_{12} = A_2 + B_2 e^{-\gamma_2 \Delta Y},$$
$$A_1 = 1.6, \quad A_2 = -1.6, \quad B_1 = -0.49, \quad B_2 = 0.6, \quad \gamma_1 = 16.67\ \text{g/J}, \quad \gamma_2 = 33.37\ \text{g/J}.$$

The initial conditions are selected as follows:

$$n_{\text{oc}}(t = 0) = 11.06\ \text{cells}, \quad n_{\text{ob}}(t = 0) = 212.13\ \text{cells}.$$

The evolution versus time of the number of osteoclasts and osteoblasts is shown in Figure 14.

The equilibrium points are obtained as follows:

$$\dot{n}_{\text{oc}}^{\text{eq}} = \dot{n}_{\text{ob}}^{\text{eq}} = 0 \quad \Rightarrow \quad \alpha_1 = 3\ \text{day}^{-1}, \quad \alpha_2 = 4\ \text{day}^{-1}, \quad \beta_1 = 0.2\ \text{day}^{-1}, \quad \beta_2 = 0.02\ \text{day}^{-1},$$
$$n_{\text{oc}}^{\text{eq}} = \left(\frac{\beta_1}{\alpha_1}\right)^{1-g_{22}/\Gamma} \left(\frac{\beta_2}{\alpha_2}\right)^{g_{21}/\Gamma}, \quad n_{\text{ob}}^{\text{eq}} = \left(\frac{\beta_1}{\alpha_1}\right)^{g_{12}/\Gamma} \left(\frac{\beta_2}{\alpha_2}\right)^{1-g_{11}/\Gamma}.$$

8 Summary and discussion

In this work, we have developed a mechanobiological model of bone remodeling involving a mineralization of bone in a moving diffuse interface separating the marrow containing all specialized cells from newly formed bone. The phase field describes the degree of mineralization within the diffuse interface at the level of individual trabeculae; it varies continuously between the lower value (no mineral) and unity (fully mineralized phase corresponding to new bone). The field equations for the mechanical, chemical, and interfacial phenomena have been written, based on the TIP. The kinetic equations for the internal variables are obtained from a pseudo-potential of dissipation. The combination of the balance equations for the microforce associated to the phase field and the kinetic equations lead to the Ginzburg–Landau equation satisfied by the phase field with a source term accounting for the dissipative microforce. The bone remodeling phenomena have been further coupled to the cell activity responsible for bone production/resorption. Simulations illus-

trating the proposed framework have been performed in a 1D situation showing the evolution of the diffuse interface separating new bone from marrow.

The present model incorporates as a novel aspect the asynchronous activity of the remodeling sites because the cellular activity is coupled to the spatio-temporal evolution of the phase field within the BMU. The analysis of strain energy effects will lead to a spatial localization of the cell activity within the BMU and deserves future work. We have shown in a simple 1D model problem of the BMU and basing on a non-dimensional writing of the local equations that the direction of the remodeling process (apposition versus resorption of mineral) is determined from the respective contribution of two energetic contributions.

A better description of the coupling between the internal stress state and the kinetics of chemical reactions will be investigated in the near future; we shall also better formalize the mineralization process in the set of governing equations. The analysis of the respective influence of mechanical and chemical energies on the remodeling velocity shall be studied in a systematic way through sensitivity analyses to the main parameters of the model. The adopted writing of the boundary value problem in non-dimensional form is a suitable prerequisite for such an analysis.

The developed modeling framework at the level of the BMU will lead to the development of a numerical platform to simulate bone remodeling coupled to cell activity due to mechanical loading in the presence of fatigue damage and cracks.

A Evaluation of the contributions to the free energy

According to the considered form of the free energy density, we evaluate the following derivatives:

$$\frac{\partial \Psi}{\partial \phi} = \frac{\partial \Psi_{\text{mech}}}{\partial \phi} + \frac{\partial \Psi_{\text{chem}}}{\partial \phi}, \quad \frac{\partial \Psi}{\partial \nabla \phi} = \frac{\partial \Psi_{\text{chem}}}{\partial \nabla \phi} = \alpha \nabla \phi,$$
$$\frac{\partial \Psi_{\text{mech}}}{\partial \phi} = \frac{1}{2}\boldsymbol{\epsilon}^e : \frac{\partial C(\phi)}{\partial \phi} : \boldsymbol{\epsilon}^e, \quad \frac{\partial \Psi_{\text{chem}}}{\partial \phi} = h'(\phi)(\Psi_B - \Psi_M) + 2\phi(\phi-1)(2\phi-1)W,$$
$$h'(\phi) = 6\phi(2\phi-1), \quad \frac{\partial C(\phi)}{\partial \phi} = C_B - C_M,$$
$$\frac{\partial \Psi_M}{\partial n_k^{\text{exch}}} = k_M(n_k^{\text{exch}} - n_0), \quad \frac{\partial \Psi_B}{\partial n_k^{\text{exch}}} = k_B(n_k^{\text{exch}} - n_0).$$

Those intermediate results are needed to specify the coupled PDEs satisfied by the phase field and chemical variables.

B Position of the interface as a function of the applied force

For a given force $F \geq 0$ applied to the BMU, we consider an interface reaching an equilibrium position at $x = h_m$. The balance of chemical and mechanical forces is written as

$$\frac{1}{2}\epsilon^e : (C_B - C_M) : \epsilon^e = (\Psi_M - \Psi_B),$$
$$\frac{1}{2}\frac{p^2}{E_x^*} + \frac{1}{2E_y^*}\left(\frac{2F}{h_m} - \sigma_m\right)^2 = (\Psi_M^* - \Psi_B^*),$$
$$\frac{1}{2E_y^*}\left(\frac{2F}{h_m} - \sigma_m\right)^2 = (\Psi_M^* - \Psi_B^*) - \frac{1}{2}\frac{p^2}{E_x^*},$$
$$\left(\frac{2F}{h_m} - \sigma_m\right)^2 = 2E_y^*\left[(\Psi_M^* - \Psi_B^*) - \frac{p^2}{E_x^*}\right].$$

The last equation gives the following condition:

$$(\Psi_M^* - \Psi_B^*) - \frac{p^2}{2E_x^*} > 0.$$

This last condition is satisfied in accordance with Figure 12 by the condition

$$0 < \frac{2F}{h_m} = \sigma_c < \sigma_m.$$

Reworking this last condition finally gives the expression of the interface height versus the applied force:

$$\sigma_c = \frac{2F}{h_m} = \sigma_m - \sqrt{2E_y^*}\sqrt{(\Psi_M^* - \Psi_B^*) - \frac{p^2}{2E_x^*}}, \quad h_m = \frac{2F}{\sigma_m - \sqrt{2E_y^*}\sqrt{(\Psi_M^* - \Psi_B^*) - p^2/(2E_x^*)}}.$$

This last expression gives a second condition at the position of the interface, $\sigma_c > 0$; thus,

$$\sigma_m > \sqrt{2E_y^*}\sqrt{(\Psi_M^* - \Psi_B^*) - \frac{p^2}{2E_x^*}}, \quad \Psi_M^* - \Psi_B^* < \frac{\sigma_m^2}{2E_y^*} + \frac{p^2}{2E_x^*}.$$

In the opposite case:

$$\frac{2F}{h_m} = 2\sigma_m - \sigma_c > \sigma_m.$$

We obtain the following expression of the interface height:

$$\frac{2F}{h_m} = \sigma_m + \sqrt{2E_y^*}\sqrt{(\Psi_M^* - \Psi_B^*) - \frac{p^2}{2E_x^*}}, \quad h_m = \frac{2F}{\sigma_m + \sqrt{2E_y^*}\sqrt{(\Psi_M^* - \Psi_B^*) - p^2/(2E_x^*)}}.$$

The two conditions on quantity $\Psi_M^* - \Psi_B^*$,

$$\frac{p^2}{2E_x^*} < \Psi_M^* - \Psi_B^* < \frac{\sigma_m^2}{2E_y^*} + \frac{p^2}{2E_x^*},$$

are here obtained for given value of the phased field ϕ and chemical term n_{exch} at the interface, considered to be the same for any position of the interface. These two conditions can be easily understood. As the mechanical term is always negative in (7.7), the chemical term that has the same sign as quantity $\Psi_M^* - \Psi_B^*$ at the interface should then be positive to ensure the possibility of remodeling. On the other side, a too large value of this quantity at the interface provides bone remodeling for $F = 0$, which contradicts observations. The range of value for the quantity $\Psi_M^* - \Psi_B^*$ leads to the possibility for F to take values into the range

$$\frac{h_m\sigma_c}{2} < F < \frac{h_m(2\sigma_m - \sigma_c)}{2},$$

in which case, bone remodeling takes place under sufficient applied stress. In any case, for a too large value of force F, our model gives a complete bone resorption behavior.

Nomenclature

Thermo-mechanical variables

$\mathbf{u}$	Displacement
$\boldsymbol{\sigma}$	Cauchy stress
$\mathbf{f}, \mathbf{t}$	Volume and surface densities of external forces
T	Temperature
q	Heat flux
$\dot{\boldsymbol{\epsilon}}^e$	Elastic strain rate
$(\cdot)^{\text{prod}}$	Quantity relative to the production of chemical species
$\dot{\boldsymbol{\epsilon}}^{\text{irr}}, \dot{\boldsymbol{\epsilon}}^{\text{irr}}_{\text{mech}}, \dot{\boldsymbol{\epsilon}}^{\text{irr}}_{\text{prod}}$	Total, mechanical, and produced irreversible strain rates
$C(\phi, T)$	Elastic stiffness tensor
C_B, C_M	Elasticity tensors of new bone and marrow
$\bar{\sigma}$	Equivalent Von Mises stress
$\Delta Y(x)$	Strain energy density

Biochemical variables

ϕ	Phase field variable (order parameter), $0 \leq \phi \leq 1$
$\pi_\phi, \pi_\phi^{\text{ext}}, \pi_\phi^{\text{cont}}$	Internal, external, and contact forces associated to ϕ
ξ_ϕ	Microforce associated to $\nabla\phi$
$\pi_\phi^{\text{nondiss}}, \pi_\phi^{\text{diss}}$	Non-dissipative and dissipative microforces
$n_k, n_k^{\text{exch}}, n_k^{\text{prod}}$	Total, exchanged, and produced number of moles of k-species
n_{k0}	Initial value of the mole fraction of k-species
$n_{k,IM}^{\text{eq}}$	Equilibrium value of the mole fraction of k-species at the bone-marrow interface
$n_{k,IM}^{\text{eq}}$	Equilibrium value of the number of moles of k-species at the bone-marrow interface
n_k^{exch}	Number of exchanged moles of k-species
$\mu_k^{\text{prod}}, \mu_k^{\text{prodext}}, \mu_k^{\text{prodcont}}$	Chemical potentials for the production, external, and contact chemical actions
$\Psi(\phi, \nabla\phi, \epsilon^e, n_k^{\text{exch}}, T)$	Free energy density
$\Omega(\pi_\phi^{\text{diss}}, \sigma, \nabla\mu_k^{\text{prod}}, \mu_k^{\text{prod}}, \nabla T)$	Dissipation potential
$L(\phi)$	Influence function
$\mathbf{J}_k$	Diffusion flux of k-species
D_M, D_B	Diffusivities of chemical species in marrow and bone
k_B, k_M	Curvature parameters
α, W	Interface parameters; $\delta \cong 2\sqrt{2\alpha/W}$ interface width
$n_{\text{ob}}(t), n_{\text{oc}}(t)$	Total numbers of osteoblasts and osteoclasts
$g_{11}, g_{12}, g_{21}, g_{22}$	Exponents expressing transduction by osteocytes
$\bar{n}_i$	Number of cells of type i at steady state
K_1, K_2	Normalized cell activities
D_{ocy}	Characteristic domain occupied by the osteocytes
R_{OC}	Radius of the influence zone for the osteocytes

References

[1] M. A. Parfitt, Osteonal and hemi-osteonal remodeling: The spatial and temporal framework for signal traffic in adult human bone, *J. Cell. Biochem.* **55** (1994), 273–286.

[2] D. W. Sommerfeldt and C. T. Rubin, Biology of bone and how it orchestrates the form and function of the skeleton, *Eur. Spine J.* **10** (2001), 86–95.

[3] H. M. Frost, The Utah paradigm of skeletal physiology: An overview of its insights for bone, cartilage and collagenous tissue organs, *J. Bon. Miner. Metab.* **14** (2001), 179–184.

[4] J. Wolff, *Das Gesetz der Transformation der Knochen*, Hirschwald, Berlin, 1892.

[5] S. C. Cowin and W. C. Van Buskirk, Surface bone remodeling induced by a medullary pin, *J. Biomech.* **12** (1979), 269–276.

[6] G. Chen, G. J. Pettet, M. Pearcy and D. L. S. McElwain, Modelling external bone adaptation using evolutionary structural optimisation, *Biomech. Model. Mechanobiol.* **6** (2007), 275–285.

[7] M. Zaidi, Skeletal remodeling in health and disease, *Nature Medicine* **13** (2007), 791–801.

[8] A. C. Allori, A. M. Sailon, P. H. Jenny and S. M. Warren, Biological basis of bone formation, remodeling, and repair. Part III: Biomechanical forces, *Tissue Eng. B* **14** (2008), 285–293.

[9] F. B. Boyce and L. Xing, Functions of RANKL/RANK/OPG in bone modeling and remodeling, *Arch. Biochem. Biophys.* **473** (2008), 139–146.

[10] P. Christiansen, The skeleton in primary hyperparathyroidism: A review focusing on bone remodeling, structure, mass, and fracture, *APMIS Suppl.* **102** (2001), 1–52.

[11] E. Seeman and P. D. Delmas, Bone quality. The material and structural basis of bone strength and fragility, *N. Engl. J. Med.* **354** (2006), 2250–2261.

[12] J. F. Ganghoffer, Mechanics and thermodynamics of surface growth viewed as moving discontinuities, *Mech. Res. Comm.* **38** (2011), 372–377.

[13] J. Sanz-Herrera, J. Garcia-Aznar and M. Doblaré, A mathematical approach to bone tissue engineering, *Acta Biomater.* **5** (2009), 219–229.
[14] J. F. Ganghoffer, Mechanical modeling of growth considering domain variation. Part II: Volumetric and surface growth involving Eshelby tensors, *J. Mech. Phys. Solids* **58** (2010), 1434–1459.
[15] J. F. Ganghoffer and J. Sokolowski, A micromechanical approach to volumetric and surface growth in the framework of shape optimization, *Int. J. Engng. Sci.* **74** (2014), 207–226.
[16] R. Hambli, Connecting mechanics and bone cell activities in the bone remodeling process: An integrated finite element modeling, *Front. Bioeng. Biotechnol.* **2** (2014), DOI 10.3389/fbioe.2014.00006.
[17] S. J. Hollister, J. M. Brennan and N. Kikuchi, A homogenization sampling procedure for calculating trabecular bone effective stiffness and tissue level stress, *J. Biomech.* **27** (1994), 433–444.
[18] M. Bagge, A model of bone adaptation as an optimization process, *J. Biomech.* **33** (2000), 1349–1357.
[19] A. Tovar, N. M. Patel, G. L. Niebur, M. Sen and J. E. Renaud, Topology optimization using a hybrid cellular automat on method with local control rules, *J. Mech. Des.* **128** (2006), 1205–1216.
[20] I. G. Jang and I. Y. Kim, Computational study of Wolff's law with trabecular architecture in the human proximal femur using topology optimization, *J. Biomech.* **41** (2008), 2353–2361.
[21] I. G. Jang and I. Y. Kim, Application of design space optimization to bone remodeling simulation of trabecular architecture in human proximal femur for higher computational efficiency, *Finite Elem. Anal. Des.* **4** (2010), 311–319.
[22] D. R. Carter, D. P. Fyhrie and R. T. Whalen, Trabecular bone density and loading history: Regulation of tissue biology by mechanical energy, *J. Biomech.* **20** (1987), 785–795.
[23] D. R. Carter, T. E. Orr and D. P. Fyhrie, Relationships between loading history and femoral cancellous bone architecture, *J. Biomech.* **22** (1989), 231–244.
[24] R. Huiskes, H. Weinans, H. J. Grootenboer, M. Dalstra, B. Fudala and T. J. Sloof, Adaptive bone-remodelling theory applied to prosthetic-design analysis, *J. Biomech.* **20** (1987), 1135–1150.
[25] G. S. Beaupré, T. E. Orr and D. R. Carter, An approach for time-dependent bone modeling and remodeling-application: A preliminary remodeling simulation, *J. Orthop. Res.* **8** (1990), 662–670.
[26] P. J. Prendergast and D. Taylor, Prediction of bone adaptation using damage accumulation, *J. Biomech.* **27** (1994), 1067–1076.
[27] R. B. Martin, A mathematical model for fatigue damage repair and stress fracture in osteonal bone, *J. Orthop. Res.* **13** (1995), 309–316.
[28] R. B. Martin, D. R. Burr and N. A. Sharkey, *Skeletal Tissue Mechanics*, New York, Springer, 1998.
[29] R. T. Hart and S. P. Fritton, Introduction to finite element based simulation of function al adaptation of cancellous bone, *Forma* **12** (1997), 277–299.
[30] C. R. Jacobs, J. C. Simo, G. S. Beaupré and D. R. Carter, Adaptive bone remodeling incorporating simultaneous density and anisotropy considerations, *J. Biomech.* **30** (1997), 603–613.
[31] P. Fernandes, H. Rodrigues and C. Jacobs, A model of bone adaptation using a global optimization criterion based on the trajectorial theory of Wolff, *Comput. Methods Biomech. Biomed. Eng.* **2** (1999), 125–138.
[32] R. Ruimerman, P. Hilbers, B. van Rietbergen and R. Huiskes, A theoretical framework for strain-related trabecular bone maintenance and adaptation, *J. Biomech.* **38** (2005), 931–941.
[33] R. Hambli, D. Soulat, A. Gasser and C. L. Benhamou, Strain-damage coupled algorithm for cancellous bone mechano-regulation with spatial function influence, *Comput. Methods Appl. Mech. Eng.* **198** (2009), 2673–2682.
[34] R. Hambli, Numerical procedure for multiscale bone adaptation prediction based on neural networks and finite element simulation, *Finite Elem. Anal. Des.* **47** (2011), 835–842.
[35] R. Hambli, K. Katerchi and C. L. Benhamou, Multiscale methodology for bone remodeling simulation using coupled finite element and neural network computation, *Biomech. Model. Mechanobiol.* **10** (2011), 133–145.
[36] T. Adachi, Y. Kameo and M. Hojo, Trabecular bone remodeling simulation considering osteocytic response to fluid-induced shear stres, *Philos. Trans. R. Soc. A* **368** (2010), 2669–2682.
[37] S. Ramtani and M. Zidi, A theoretical model of the effect of continuum damage on a bone adaptation model, *J. Biomech.* **34** (2001), 471–479.
[38] L. M. McNamara and J. P. Prendergast, Bone remodeling algorithms incorporating both strain and microdamage stimuli, *J. Biomech.* **40** (2007), 1381–1391.
[39] C. J. Hernandez, G. S. Beaupre and D. R. Carter, A model of mechanobiologic and metabolic influences on bone adaptation, *J. Rehabil. Res. Dev.* **37** (2000), 235–244.
[40] C. J. Hernandez, G. S. Beaupre, T. S. Keller and D. R. Carter, The influence of bone volume fraction and ash fraction on bone strength and modulus, *Bone* **29** (2001), 74–78.
[41] R. Huiskes, R. Ruimerman, G. H. van Lenthe and J. D. Janssen, Effects of mechanical forces on maintenance and adaptation of formin trabecular bone, *Nature* **405** (2000), 704–706.
[42] S. J. Hazelwood, R. B. Martin, M. M. Rashid and J. J. Rodrigo, A mechanistic model for internal bone remodeling exhibits different dynamic responses in disuse and overload, *J. Biomech.* **34** (2001), 299–308.
[43] D. Taylor and T. C. Lee, Microdamage and mechanical behaviour: Predicting failure and remodeling in compact bone, *J. Anat.* **203** (2003), 203–211.

[44] D. Taylor, E. Casolari and C. Bignardi, Predicting stress fractures using a probabilistic model of damage, repair and adaptation, *J. Orthop. Res.* **22** (2004), 487–494.
[45] J. M. Aznar, T. Rueberg and M. Doblare, A bone remodeling model coupling microdamage growth and repair by 3DBMU-activity, *Biomech. Model. Mechanobiol.* **4** (2005), 147–167.
[46] K. Tsubota, Y. Suzuki, T. Yamada, M. Hojo, A. Makinouchi and T. Adachi, Computer simulation of trabecular remodeling in human proximal femur using large-scale voxel FE models: Approach to understanding Wolff's law, *J. Biomech.* **42** (2009), 1088–1094.
[47] Y. Matsuura, S. Oharu, T. Takata and A. Tamura, Mathematical approaches to bone reformation phenomena and numerical simulations, *J. Comput. Appl. Math.* **158** (2003), 107–119.
[48] Y. Matsuura, S. Oharu and D. Tebbs, On a class of reaction-diffusion systems describing bone remodeling phenomena, *Nihonkai Math. J.* **13** (2002), 17–32.
[49] K. Tezuka, Y. Wada and M. Kikuchi, iBone: A reaction diffusion based shape optimization method, *Key Eng. Mater.* **243/244** (2003), 601–606.
[50] K. Tezuka, Y. Wada, A. Takahashi and M. Kikuchi, Computer-simulated bone architecture in a simple bone remodeling model based on a reaction-diffusion system, *J. Bone Miner. Metab.* **23** (2005), 1–7.
[51] S. V. Komarova, R. J. Smith, S. J. Dixon, S. M. Sims and L. M. Wahl, Mathematical model predicts a critical role for osteoclasts autocrine regulation in the control of bone modelling, *Bone* **33** (2003), 206–215.
[52] C. Rattanakul, Y. Lenbury, N. Krishnamara and D. J. Wollkind, Modeling of bone formation and resorption mediated by parathyroid hormone: Response to estrogen/PTH therapy, *Biosystems* **70** (2003), 55–72.
[53] A. Moroz, M. C. Crane, G. S. David and I. Wimpenny, Phenomenological model of bone remodeling cycle containing osteocyte regulation loop, *Biosystems* **84** (2006), 183–190.
[54] V. Lemaire, F. L. Tobin, L. D. Greller, C. R. Cho and L. J. Suva, Modelling the interactions between osteoblasts and osteoclasts activities in the bone remodeling, *J. Theor. Biol.* **229** (2004), 293–309.
[55] S. Maldonado, R. Findeisen and F. Allgöwer, Mathematical modeling and analysis of force induced bone growth, in: *Proceedings of the 28th International Conference of IEEE-EMBC* (New York 2006), 3154–3160.
[56] M. D. Ryser, N. Nigam and S. V. Komarova, Mathematical modeling of spatio-temporal dynamics of a single bone multicellular unit, *J. Bone Miner. Res.* **24** (2009), 860–870.
[57] P. Pivonka, J. Zimak, D. W. Smith, B. S. Gardiner, C. R. Dunstan, N. A. Sims, T. J. Martin and G. R. Mundy, Model structure and control of bone remodeling: A theoretical study, *Bone* **43** (2008), 249–263.
[58] N. Bonfoh, E. Novinyo and P. Lipinski, Modeling of bone adaptive behavior based on cells activities, *Biomech. Model. Mechanobiol.* **5** (2011), 789–798.
[59] I. Steinbach, Phase field models in materials science, *Model. Simul. Mater. Sci. Eng.* **17** (2009), 1–31.
[60] H. Emmerich and R. Travasso, Phase-field simulations: Materials science meets biology and medicine, *Philos. Mag.* **91** (2011), 1–2.
[61] K. Ammar, B. Appolaire, C. Cailletaud, F. Feyel and S. Forest, Finite element formulation of a phase field model based on the concept of generalized stresses, *Comp. Mater. Sci.* **45** (2009), 800–805.
[62] E. Fried and M. Gurtin, Continuum theory of thermally induced phase transitions based on an order parameter, *Phys. D* **68** (1993), 326–343.
[63] M. Gurtin, Generalized Ginzburg–Landau and Cahn–Hilliard equations based on a microforce balance, *Phys. D* **92** (1996), 178–192.
[64] I. Goda, M. Assidi and J. F. Ganghoffer, A 3D elastic micropolar model for vertebral trabecular bone from lattice homogenization of the trabecular structure, *J. Mech. Beh. Biomed. Mater.* **13** (2014), 53–83.
[65] K. Ammar, B. Appolaire, C. Cailletaud and S. Forest, Combining phase field approach and homogenization methods for modelling phase transformation in elastoplastic media, *Eur. J. Comp. Mech.* **18** (2009), 485–523.
[66] K. Ammar, B. Appolaire, C. Cailletaud and S. Forest, Phase field modeling of elasto-plastic deformation induced by diffusion controlled growth of a misfitting spherical precipitate, *Philos. Mag. Lett.* **91** (2011), 164–172.
[67] K. Ammar, B. Appolaire, S. Forest, M. Cottura, Y. Le Bouar and A. Finel, Modelling inheritance of plastic deformation during migration of phase boundaries using a phase field method, *Meccanica* **49** (2014), 2699–2717.
[68] R. L. Duncan and C. H. Tuner, Mechanotransduction and the functional response of bone to mechanical strain, *Calcified Tissue Int.* **57** (1995), 344–358.
[69] J. L. Gibson, Biomechanics of cellular solids, *J. Biomech.* **38** (2005), 377–399.